A Higher Density VLBI Catalog for Navigating Magellan and Galileo

J. S. Ulvestad, O. J. Sovers, and C. S. Jacobs

Tracking Systems and Applications Section

The density of radio sources near the ecliptic in the astrometric JPL Very Long Baseline Interferometry (VLBI) catalog has been increased by over 50 percent since 1985. This density increase has been driven by the need for more sources for the VLBI navigation of the Magellan and Galileo spacecraft, but the sources also will be usable for Mars Observer and other future missions. Since the last catalog, including observations made through 1985, was published in 1988, a total of 21 radio sources has been added that fulfill the following criteria: (1) they lie within 10 deg of the ecliptic plane; (2) their correlated flux densities are above 0.2 Jy on at least one of the Deep Space Network intercontinental baselines at both 2.3 and 8.4 GHz; and (3) the source positions are known to better than 5 milliarcseconds (25 nanoradians). The density of such sources in the catalog has been increased from 15.6 per steradian to 25.2 per steradian. Ten more sources have been added that fulfill the last two criteria given above and lie between 10 deg and 20 deg from the ecliptic plane.

Analysis shows that there may be ~70 more sources with correlated flux densities above 0.2 Jy that are within ~20 deg of the ecliptic. However, VLBI navigation observations of the new and prospective sources with the 250-kHz bandwidth of the current operational system will require the use of two 70-m antennas in most cases. Including both old and new sources, if two 34-m antennas are used, there will be usable navigation sources within 10 deg of a spacecraft in only 30 percent of the ecliptic, and sources within 20 deg of a spacecraft over 70 percent of the ecliptic. If one 70-m antenna were used along with a 34-m telescope, or if a somewhat wider bandwidth system such as the Mark II VLBI system (effective bandwidth of 1.8 MHz) were used with two 34-m antennas, usable navigation sources would be within 10 deg of a spacecraft over about 65 percent of the ecliptic. Within 20 deg of a spacecraft, usable sources would exist over 98 percent of the ecliptic.

I. Introduction

The technique of Very Long Baseline Interferometry (VLBI) is used to produce astrometric catalogs of the positions of compact extragalactic radio sources (generically referred to here as quasars). The catalogs are produced by making radio interferometric observations of compact radio sources and performing multiparameter fits, one output of which is a catalog of radio-source positions in a specified reference frame (e.g., [1,2]). Such a catalog can be

used for a variety of purposes, including monitoring of the Earth's orientation, measurement of plate tectonic motion, and navigation of interplanetary spacecraft. This article concentrates on the last use. Specifically, it addresses the problem of increasing the density of objects in the JPL VLBI catalog in regions of the sky that are important for planetary missions.

The general intent of the work described here has been to increase the density of sources in the catalog near the ecliptic, a great circle on the sky which approximates the path followed by all the planets in the solar system. In a technique called ΔVLBI that is used for spacecraft navigation, successive observations are made of the spacecraft and a quasar, with observables differenced to reduce errors. For navigation of a spacecraft using ΔVLBI, it is desirable to have at least one reference radio source near the spacecraft position at all times. Several different errors grow with increasing spacecraft/radio-source angular separation, so the smallest possible separations are desired. The maximum acceptable separation depends on the error budget and on the VLBI observable used. Errors grow rapidly with separation for interferometric delay measurements, but delay-rate measurement errors at the present time are dominated by wet troposphere fluctuations, which do not depend very strongly on spacecraft/quasar separation. A traditional goal has been to always have a reference source within 10 deg of the spacecraft being navigated.[1] A more accurate method of VLBI navigation is being developed [3]; it relies upon having several radio sources in approximately the same direction (to within about 30 deg), meaning that a high and moderately uniform VLBI source density is desirable along a spacecraft trajectory.

A spacecraft traveling to an outer planet may stay in a small part of the ecliptic for years. For example, the Voyager 2 spacecraft traversed less than 10 percent of the ecliptic on its 3.5-year trip from Uranus to Neptune. In such a case, the increased density of navigation reference sources is needed in only a fraction of the ecliptic. However, an inner planet mission, such as that of Magellan to Venus, may traverse the entire ecliptic in about a year. Then it is desirable to increase the density of sources all along the ecliptic. In the JPL VLBI catalog published in 1988 [1], the density of radio sources usable for navigation and within 10 deg of the ecliptic was 15.6 per steradian. Since the Magellan spacecraft will reach Venus in 1990, it was important to increase the density of the VLBI catalog before Magellan would go into orbit around Venus and

begin its radar mapping of the planet's surface. Thus, the immediate motivation for the work described here has been to prepare a new catalog for Magellan, although there are also benefits to Galileo, Mars Observer, and other upcoming missions.

This article describes the work done in recent years to increase the density of the JPL VLBI catalog in selected regions. Section II summarizes detection limits and looks briefly at some of the strategies employed for finding new candidate sources for the VLBI catalog. Section III describes VLBI experiments that have been done to check out these candidates as well as the analysis of source strength information. Section IV gives the end product of those experiments, with a catalog of positions and measured correlated flux densities for the sources. The distribution of sources along the ecliptic as a function of source strength is explored in some detail. Section V analyzes the prospects for finding more sources, and Section VI summarizes the main points of this article.

II. Hunting for More Ecliptic Plane Sources
A. Correlated Flux Density Detection Levels

If infinitely weak natural radio sources could be observed, the density of VLBI sources in the JPL catalog could be (almost) arbitrarily high and would be limited primarily by the time available for making VLBI observations and reducing the data. However, there are limitations imposed by nature and by the ground observing systems. Radio antennas have finite size as well as instrumental noise. They observe in the presence of other noise sources such as sky and ground radiation, and they have a limited observing bandwidth. Hence there is a calculable detection limit for the radio sources. Reference [4] contains some discussion of candidate identification and detection limits, and the reader is referred to that article for further information. The nominal detection limits for correlated flux density with the operational 250-kHz-bandwidth navigation VLBI system[2] (the "Block I" system) are ~0.2 Jy for two 70-m Deep Space Network (DSN) antennas, ~0.4 Jy for a baseline between a 70-m and a high-efficiency 34-m antenna, and ~0.8 Jy for two 34-m antennas.[3] Such correlated flux densities are needed at both 2.3 GHz and 8.4 GHz observing frequencies. These limits were derived for specific signal-to-noise requirements; they assumed sys-

[1] J. B. Thomas, "An Error Analysis for Galileo Angular Position Measurements with the Block I ΔDOR System," JPL Engineering Memorandum 335-26 (internal document), Jet Propulsion Laboratory, Pasadena, California, November 11, 1981.

[2] J. S. Border, "An Error Analysis for Magellan Differential Delay Rate Measurements," JPL Enginering Memorandum 335-96 (internal document), Jet Propulsion Laboratory, Pasadena, California, February 23, 1987.

[3] The unit of flux density, the jansky (Jy) is equal to 10^{-26} $W \cdot m^{-2} \cdot Hz^{-1}$.

tem temperatures of 35 K (system temperature is a measure of the noise contributed by the telescope, receivers, and background), aperture efficiencies of ~60 percent, and a 250-kHz observing bandwidth. The 34-m antennas currently have higher system temperatures at 2.3 GHz than previously envisioned, so the correlated flux density limits at this frequency may be significantly (~20–30 percent) higher than the numbers given above for baselines involving 34-m antennas.

In considering the suitability of radio sources for the catalog, it is important to recognize that the relevant measure of source strength is the *correlated* flux density, which is always less than or equal to the *total* flux density. The correlated flux density is a measure of the strength of the part of the radio source that causes well-defined interference between the two telescopes making up an interferometer. For a point radio source, the correlated flux density is equal to the total flux density. However, for a more extended source, the correlated output of an interferometer is reduced because of the superposition of electromagnetic waves coming from more than one direction in the sky, which washes out the interference pattern. A priori, the correlated flux density can have any value between zero and the total flux density for a given radio source. There are no quantitative predictions of the expected distribution of the ratio between correlated and total flux densities, although it is known that certain classes of sources have, on average, a higher fraction of correlated flux density than other sources (see [4] for further discussion).

B. Lists of Candidate Sources

The best candidate sources for the JPL VLBI catalog have been selected and sieved over a number of years in the process of building that catalog, with particular emphasis on candidates near the ecliptic (e.g., [5]). In order to increase the catalog density in any region, more marginal candidates must be considered. In general, this means testing radio sources with lower total flux densities and/or with spectral flux distributions that are less likely to indicate a high ratio of correlated to total flux density. Because these are marginal candidates, the investment in antenna time and human time is large for each usable source that is found and observed enough to get an accurate position. Thus, the task of finding new sources is limited ultimately by the resources available as much as by the lack of candidate sources; at some point, the effort required to examine rather poor candidate sources becomes too great for the meager return expected.

Reference [4] outlines the basic method of finding new candidate radio sources. Because of the need to find sources for Magellan rather quickly, the step of searching

through single-telescope surveys was not done specifically for the work described in this article. Instead, emphasis was placed on objects that already had been observed interferometrically, had positions accurate to an arcsecond or better, and showed some promise of containing compact radio components of substantial strength. These objects came predominantly from two sources. First, there are lists of radio sources previously surveyed with intercontinental baselines in the DSN [4–7]. Many of these observations were made to find candidates for the VLBI catalog, but they were not followed up systematically, especially at the low end (0.2–0.5 Jy) of the correlated flux density scale. A second, smaller list of sources was selected from a survey of compact, low-frequency radio sources near the galactic center and anti-center [8]; these are the regions where the ecliptic and galactic planes intersect. Very Large Array (VLA) observations of these objects by one of the authors (J. S. Ulvestad) together with A. P. Rao and S. Ananthakrishnan of the Tata Institute of Fundamental Research provided a few more compact radio sources that were tried on intercontinental baselines.

III. Experiments and Data Analysis

The new candidate sources for the VLBI catalog have been observed in some of the regular DSN intercontinental VLBI experiments (Goldstone–Canberra or Goldstone–Madrid baseline) for catalog maintenance and enhancement, from mid-1986 through early 1989. The observations and analysis of such experiments are detailed in other papers describing the JPL VLBI catalog, such as [1]. All observations were dual-frequency, employing multiple frequency channels at S-band (2.3 GHz) and at X-band (8.4 GHz) in order to allow accurate delay measurements. The new data were processed using the JPL/Caltech Block II VLBI correlator described in [9]. This article reports results from the first extended usage of that correlator in the VLBI catalog effort. The bulk of the data was taken with the Mark II VLBI recording system [10], but two experiments are included which used the Mark III systems [11] that were installed recently in the DSN.

In the recent experiments, whose usable lengths ranged from ~8 to ~24 hours, a number of new candidate sources were observed, together with many of the objects already in the VLBI catalog. In this way, positions of the new sources were tied to the existing radio reference frame. For sources near the celestial equator, which includes most objects near the ecliptic, a baseline with a large north-south component is needed to get accurate source declinations. Thus, experiments on the DSN baseline between Goldstone and Canberra were quite important, since the

Goldstone–Madrid baseline gives poor north–south resolution.

The primary quantity of interest for the VLBI catalogs always has been the astrometric source positions. However, the correlated flux densities also are crucial for determining the suitability of radio sources for spacecraft navigation. Since the VLBI catalog experiments employ a larger bandwidth (effectively 1.8 MHz for Mark II, and up to 56 MHz for Mark III) than the 250 kHz of the Block I navigation system, these experiments can determine positions for sources that are not strong enough to be usable for navigation. Knowledge of the correlated flux densities and their variability with time and projected baseline gives information about which sources can be used for certain antenna combinations in order to get useful navigation data.

Correlated flux densities were estimated from the experiments between mid-1986 and late 1988. These were all Mark II VLBI experiments; there is not yet a working system to find correlated flux densities from Mark III catalog experiments. Initial values were determined by taking the measured correlation coefficients and calculating the correlated flux densities using the best available values for antenna gains (e.g., [12, 13]) and system temperatures. In most cases at X-band and some at S-band, system temperature measurements were read from strip charts. If no such data were available, zenith system temperatures were used along with a crude model for variation with elevation angle in order to get system temperatures for each observation. In such instances, an estimate of the total flux density of each source at both frequencies was used to determine the source's contribution to the system temperature.

Since there was no explicit amplitude calibration done for the VLBI experiments, it was necessary to make consistency checks for the set of experiments used in the correlated flux density analysis. The most straightforward check was based on the fact that most compact radio sources vary in strength, but the variations of different sources are completely independent. Therefore, in comparing any two experiments, half the sources should show increases in their correlated flux densities and half should show decreases.[4]

For each source in every experiment, an average correlated flux density was determined, usually from 2–4 measurements. Pairs of experiments using the same two DSN

complexes were compared by taking ratios of the average correlated flux densities at each frequency for each source common to both experiments. If the median value of the correlated-flux-density ratio at one of the frequencies was near 1.0, the experiment flux-density scales were considered consistent for that observing frequency; if it differed from 1.0 by more than 10–15 percent, the calibration of the two experiments was investigated further. In some cases, the choice of a different frequency channel (three were available at each band) resolved the discrepancy, implying that a particular experiment had an anomalous gain in one channel (e.g., due to mistuning of the maser receiving bandpass). In other instances, the "measured" system temperatures were lower than the zenith temperatures for some observations, implying that strip charts were miscalibrated or had changing calibration during an experiment. In these cases, the zenith system temperature and the crude atmospheric model were used to calculate the system temperature during a given observation, and these revised values sometimes brought the correlated flux density scales into agreement. Some experiments could never be brought into agreement and were discarded from the correlated flux density data set; for several experiments, the X-band amplitude data were discarded, but the S-band data were kept. Possible causes for these outlier experiments included poor antenna pointing (more important at X-band) and system gain variations.

The final flux-density data base included ten experiments on the Goldstone–Canberra baseline and ten on the Goldstone–Madrid baseline. Seven of those 20 experiments had little or no usable X-band flux-density data. A few individual observations were deleted from the experiments because of transient or short-term instrumental problems. Judging by the median correlated flux densities, final amplitude scales varied by ±10 percent at S-band and as much as ±15 percent at X-band. These are also the approximate errors on individual measurements, as estimated from the repeatability of measurements on sources observed at the same hour angle on two consecutive days. Estimated correlated flux density errors for individual source observations are found by adding ∼0.03 Jy system noise in quadrature to 15 percent (at S-band) or 20 percent (at X-band) of the total correlated flux density. The 15 percent and 20 percent values, in turn, are roughly the scale errors and individual measurement errors added in quadrature. Errors in the *average* flux densities are somewhat fewer, but cannot be quantified simply for the general case. They depend on the details of observations for each source; for example, errors on different observations of a source in a single experiment can be highly correlated, because they reflect the same scale error in addition to (possibly) uncorrelated errors in system noise temperature and antenna pointing.

---

[4] Source structure causes correlated flux densities to vary with time in a given experiment. However, in the absence of deliberate attempts to observe sources at times of minimum (or maximum) correlated flux density in a given experiment, structure should cause no overall trends for flux densities to be higher or lower in one experiment than in another.

IV. Results

Table 1 presents the astrometric data for a new VLBI catalog (the 1989-5 catalog) with a higher density of sources near the ecliptic. The source positions are given in the J2000 system, with the reduction to that system described more completely in [1].[5] In this table, only those sources with formal declination errors less than five milliarcseconds (25 nanoradians) are included; such uncertainties are within the error budgets specified for Magellan and Galileo. There are 166 radio sources listed in this table. In contrast, the catalog published in [1] (1987-1) had only 105 radio sources with formal declination errors smaller than five milliarcseconds; the number of sources with accurate positions has grown by nearly 60 percent. Most of the new sources are near the ecliptic plane, as described later in this section.

Tables 2 and 3 contain the best estimates of the correlated flux densities of the radio sources listed in Table 1, from experiments between June 1986 and September 1988. The X-band data on the Madrid baseline come from experiments since May 1987, because the two 1986 experiments did not produce usable X-band amplitude data. No correlated flux densities are listed for objects for which there are no reliable amplitude data in the experiments between mid-1986 and late 1988. Since the source structures cause different correlated flux densities on different baselines, results are listed separately for the Goldstone–Canberra and Goldstone–Madrid baselines. At each frequency on each baseline, the tables give the average correlated flux densities, root-mean-square (RMS) variation of the correlated flux density measurements, maximum and minimum correlated flux density values, and the number of individual observations used to derive those numbers. Error estimates for individual observations were described in Section III, and are roughly 15 percent at S-band and 20 percent at X-band (plus 0.03 Jy added in quadrature at each frequency). Errors in the average flux densities are somewhat smaller, but are not quantified easily.

The catalog sources have been classified based on their suitability for VLBI navigation using different antenna pairs. Because of the higher system temperatures of the 34-m antennas at S-band, the correlated flux density cutoffs for different antenna pairs have been adjusted from those given in Section II. Category 1 sources typically have at least 0.8 Jy of correlated flux density at X-band and 1.0 Jy at S-band, so they should be usable for navigation with the

Block I system on baselines with two 34-m high-efficiency antennas. Sources in category 2 typically have correlated flux densities between 0.4 and 0.8 Jy at X-band, or 0.5 and 1.0 Jy at S-band, indicating that at least one 70-m antenna should be used for VLBI navigation. Category 3 sources have typical correlated flux densities in the 0.2–0.4 Jy (X-band) or 0.2–0.5 Jy (S-band) range, requiring 70-m pairs for navigation observations. Objects that are likely to be weaker than 0.2 Jy, and currently unusable for VLBI navigation, are relegated to category 4.

Table 4 gives the flux-density classifications for all the accurately positioned sources listed in Table 1. Classifications are given separately at S-band and X-band for most sources. The criteria for inclusion in a specific class are that the average correlated flux density, and at least 75 percent of the correlated flux densities from individual observations, are above the cutoff value for a given class. A "net" class for dual-frequency observations is also given; if the S-band and X-band classes differ, as they often do, this number is the larger of those given for the individual frequencies. Tabulating the separate values for the different frequencies as well as this dual-frequency classification facilitates selection of sources for single-frequency VLBI observations and also gives information on which band is likely to give the most trouble in dual-frequency data. Separate listings are given for each baseline (Goldstone–Canberra and Goldstone–Madrid), since radio source structure makes the correlated flux densities differ significantly between the two baselines. For some sources, the information in Table 4 is incomplete because there may not be correlated flux density values at both frequencies on both baselines in the experiments considered here. In those cases, older correlated flux density results (e.g., [5–7]) or values from the other baseline have been used to estimate a dual-frequency classification, which is included in Table 4 in parentheses.

It is crucial to recognize that many of the sources in the VLBI catalog are variable in strength on time scales on the order of a year, some by a factor of two or more. Therefore, 2- or 3-year-old correlated flux densities do not necessarily reflect current values. Some effort has been made to take variability and source structure into account by requiring that at least 75 percent of the observations have correlated flux densities above the cutoff for a certain class for inclusion in that class. Still, a source that is in the highest of the above-defined flux density categories based on its strength in 1988 may not be in that category when it is to be used for Magellan navigation in 1990 or 1991, so it may no longer be suitable for two 34-m antennas. It is hoped that more up-to-date correlated flux density values will be available when the Magellan orbital phase begins

---

[5] Note that the full catalog accuracy for navigation can be achieved only via careful consideration of the reference frames in use for the radio source catalog, spacecraft navigation, and planetary ephemerides.

in August 1990, but there always will be enough of a time lag between amplitude measurements and navigation usage that sources can vary significantly.

Figures 1–3 show histories of correlated flux densities for several radio sources in the 1986–1988 period. In these figures, the correlated flux densities are plotted against interferometer hour angle (IHA). The IHA is the source hour angle with respect to the local meridian at the midpoint in longitude between the two observing stations. Figures 1(a) and 1(b) are plots of the quasar P 0420−01 at X-band on the Goldstone–Canberra and Goldstone–Madrid baselines, respectively. Note the decrease in correlated flux density by a factor of 3 or more between 1986 and 1988. Although it is more than 20 deg from the ecliptic, this source is a strong candidate for ΔVLBI navigation when Magellan is in the vicinity and two 34-m antennas are employed. P 0420−01 is listed in category 1, but there is no guarantee that it will be that strong in 1990 and 1991, as the past flux variability shows.

Figures 2(a) and 2(b) show the source P 1510−08 at both bands on the Goldstone–Madrid baseline. Its S-band correlated flux density increased by a factor of 3 or more between 1986 and 1988, which was sufficient to move it from class 2 to class 1. For part of the Magellan cruise VLBI campaign in early 1990, this is the best source visible on the Madrid baseline. If its flux density is the same as in 1986, it will not be detectable at S-band with a 34-m pair, and there would be *no* usable sources for the Goldstone–Madrid baseline when two 34-m antennas are used. Although on the average, as many sources increase in flux as decrease, practical limitations mean that *unmonitored* variability can only reduce the number of sources presumed to be available in a given flux density category. If five sources decrease in strength to drop out of class 1, and five quasars increase to move into that category, the increases do little good because there is no way of knowing which five sources can now be observed with smaller antennas.

Figures 3(a) and 3(b) show correlated flux density plots for a weaker radio source, 0536+145, at X-band on each of the two baselines. Note the different correlated flux densities on each baseline, which illustrate the reason that sources can have different flux density classifications on the two baselines. Inspecting Fig. 3(b), it is evident that a modest decrease in the flux density for 0536+145 can be enough to move it below the dividing line between class 2 and class 3 sources, so it is impossible to predict whether two 70-m antennas would be needed for this source at a given time.

Figures 4–6 display results of successive cuts on the sources in Table 1, based on their strength on the Goldstone–Canberra baseline. These plots show source positions over the part of the celestial sphere between −40 and 40 deg declination, with 10-degree-radius circles drawn around each source position. In each plot, the ecliptic is shown as a sinusoidal curve.

There are 120 sources in categories 1, 2, and 3 on the Goldstone–Canberra baseline; i.e., 120 catalog sources are observable with two 70-m antennas using the Block I VLBI system. All 76 of them within 20 deg of the ecliptic, as well as some others in the plotted declination range, are shown in Fig. 4. Good sky coverage has been achieved, with significant "holes" along the ecliptic only at 3^h–5^h and 16^h–19^h right ascension, and a less prominent source deficit near 10^h right ascension. Considerable effort has been expended in the last several years to fill in the 3^h–5^h hole, but most of the new sources added to the catalog in that region are slightly weaker than 0.2 Jy most of the time. The 16^h–19^h region is where the ecliptic intersects the galactic plane near the galactic center. Confusion with galactic radio sources, and the consequent lack of source surveys in the region, make it difficult to find candidate VLBI sources.

Figure 5 is based on the 58 sources in categories 1 and 2, including 33 within 20 deg of the ecliptic. Note the generally sparser sky coverage. Figure 6 is based on the 18 sources in category 1 on the Canberra baseline, eight of which are within 10 deg of the ecliptic. This plot shows the inadvisability of navigating a spacecraft all the way around the ecliptic using only 34-m antenna pairs with the Block I system. For instance, the *only* usable sources within 15 deg of the ecliptic in the 0^h–12^h range of right ascension are P 0112−017 (a new source added since the last catalog was published) and OJ 287. In total, there will be a source within 10 deg of a spacecraft over only ∼30 percent of the ecliptic.

Similar plots have been made for the Goldstone–Madrid baseline but are not included here. Their general appearance is similar to those for the Canberra baseline, except the hole near 16^h–19^h right ascension is worse because of the inability to observe sources below −26 deg declination. In general, the observations in this region also are constrained much more by the limited view periods for both spacecraft and quasar. For example, a source 15 deg east of the spacecraft at −22 deg declination may not be visible immediately following (and certainly not before) a VLBI observation of the spacecraft.

Figure 7 shows the same sources as does Fig. 6, but with the circles around the quasars expanded to 20 deg radius. Clearly, even if quasars as much as 20 deg from

the spacecraft are deemed acceptable, there are still significant holes in the source distribution for observations using 34-m pairs. About 70 percent of the ecliptic has a usable reference source within 20 deg. Increasing the allowable spacecraft/quasar separation to 25 deg would give coverage to approximately 90 percent of the ecliptic.

Since the strongest sources were in the catalog regardless of their ecliptic latitude, the density increase since the last published catalog has been confined almost entirely to the category 2 and 3 sources. The number of category 1, 2, and 3 sources (on at least one baseline) within 10 deg of the ecliptic has increased by 21 since the last published catalog, corresponding to a 60 percent density increase, from 15.6 to 25.2 per steradian. Another ten sources have been added between 10 deg and 20 deg of the ecliptic, and six more sources were added slightly farther to the north of the ecliptic in the direction near that of the galactic center. Thus, a total of 37 of the 43 new class 1, 2, and 3 sources added since the 1987-1 catalog facilitate navigation near the ecliptic plane. Figure 8 illustrates the change in the catalog; it is a version of Fig. 4 without circles surrounding each source position, and with the old and new sources indicated by different symbols.

V. Directions for Future Work

A. Source Lists and Surveys

In the effort to find yet more VLBI navigation sources, the radio source surveys in the astronomical literature have been studied systematically. This effort was similar to that described in [4], but some newer surveys and a much lower flux density limit were used. A list has been compiled that includes over 2,000 radio sources within ~20 deg of the ecliptic plane. The primary selection criterion is that these sources have total flux densities above ~0.25 Jy at an observing frequency of 5 GHz, although some sources have been selected from surveys at 2.7 GHz (e.g., [14]) or 1.4 GHz [15]. For the regions between −0.5 deg and 19.5 deg declination (except for the areas near the galactic plane), the MIT-Green Bank 5-GHz survey [16] has a completeness limit well below 0.25 Jy; the surveys in other areas generally are not complete to the desired selection limit. The summary list contains flux densities at several different frequencies when they are available, since spectral curvature is such an important indicator of source compactness. Table 5 shows a portion of this global source list. The literature also has been searched for all published interferometric observations of the radio sources in the large finding list, and lists have been compiled that summarize those observations. These databases are extremely useful in finding the best of the many candidate sources for possible VLBI observations in the future.

Depending on the degree of satisfaction with the current source density in the VLBI catalog, there are several options for finding more sources. The first is to use the above-described source lists to find the best candidates in some of the low-density regions of the catalog near the ecliptic plane, make moderately short baseline interferometric observations of those objects, and then try intercontinental VLBI on the sources that are still viable candidates. The area near 10^h right ascension is an obvious candidate for this procedure. Because of the confusion problem near the galactic center and the lack of prior surveys, the area near 18^h right ascension does not lend itself easily to such a screening procedure. Most of the known candidates in that area have been examined already. If a higher density of sources is desired, it may be necessary to perform a new source survey in the direction of the galactic center, probably using a short-baseline interferometer rather than a single telescope. After such a survey is made and the data analyzed, the standard post-survey screening procedures could be used. Doing a new source survey, even of this limited region, would require considerable resources, and must begin fairly soon in order to produce usable navigation radio sources by the time Galileo reaches Jupiter in 1995.

B. Expected Numbers of Sources That Could Be Added to the Catalog

Before any further efforts are made to find new VLBI catalog sources, it is useful to estimate the probabilities for finding new sources with adequate correlated flux densities for ΔVLBI navigation. In this connection, consider the distribution of sources currently in the JPL VLBI catalog. For brevity, only the Goldstone–Canberra baseline is examined here; the results are similar for the Goldstone–Madrid baseline. Since the most comprehensive source searches for the JPL VLBI catalog have been made near the ecliptic, assume for the sake of argument that *all* class 1 sources that are within 10 deg of the ecliptic are already in the VLBI catalog. Further, *assume* that the source density N as a function of correlated flux density S_c follows the relation

$$N(S_c > S_0) = N_0(S_c/S_0)^{-1.5}$$

where N_0 is the source density at correlated flux density S_0. This relation is approximately true of source counts as a function of *total* flux density above 0.1 Jy, e.g., [17]; the assumption that it also holds for *correlated* flux density is arbitrary.

Given the numbers of sources in class 1 at S and X-bands, the above relation has been used to predict the numbers of class 2 and class 3 sources at each frequency.

Predictions for the combined (dual-frequency) class also have been made, although these are more uncertain because of the different flux density limits at the two frequencies. The predictions for class 2 sources match the observations quite well at X-band and for the dual-frequency category, while the S-band predictions are low by slightly more than one standard deviation. This provides some confidence that the above assumption about the number versus correlated flux density relation is not too far from reality. For dual-frequency observations, ~75 sources are predicted to be present in classes 1–3, but the VLBI catalog contains only 50. Hence there is a deficit of ~25 sources above 0.2-Jy correlated flux density; most of these would be category 3 sources that are not in the catalog.

Since the ecliptic is not a preferred region for the extragalactic radio sources used for VLBI navigation, the source density in each class should be similar at all ecliptic latitudes. Therefore there should be ~75 class 1, 2, and 3 sources between 10 deg and 20 deg from the ecliptic plane, whereas the current VLBI catalog has only 26. As many as 50 sources may be "missing" here, including 10 from categories 1 and 2 and close to 40 from category 3.

Under the assumptions given above, the result is that ~70 sources with correlated flux densities above 0.2 Jy at S-band and at X-band conceivably could be added to the JPL VLBI catalog at distances less than 20 deg from the ecliptic. If one were to assume that $N(S_c) \propto S_c^{-1.2}$, which is the shallowest possible relation allowed by the dual-frequency correlated flux density counts between categories 1 and 3 in the region within 10 deg of the ecliptic, only ~25 sources would be missing in the annulus between 10 deg and 20 deg from the ecliptic plane. This must be the *minimum* number of sources in classes 1–3 that are within 20 deg of the ecliptic and remain to be included in the VLBI catalog. The real source deficit probably is much closer to the original estimate of 70 objects.

The list of currently known candidate sources with over ~0.25 Jy total 5-GHz flux density and within ~20 deg of the ecliptic (see previous subsection) numbers ~2,200. This is about the number expected at 5 GHz within 20 deg of the ecliptic. (The fact that some sources are missing because deep surveys have not covered the entire region is balanced by the inclusion of sources selected at lower frequencies that would not make the flux-density cutoff at 5 GHz.) Of the ~2,200 sources mentioned above, ~1,200 have published interferometric (usually VLBI or VLA) observations. Finding a significant fraction of the ~70 missing sources would require interferometric observations of most of the remaining 1,000 objects as well as new source surveys in the regions where the ecliptic and galactic planes

intersect. Since most such sources will be observable only with two 70-m antennas in the current navigation VLBI system, such extensive searches would be useful only if (1) two 70-m antennas were to be used frequently for the navigation VLBI, or (2) a wider bandwidth VLBI system were used for navigation.

VI. Summary

A new JPL VLBI catalog has been presented here that has an increased density of radio sources near the ecliptic. The coordinate system of the catalog presented here has been based on an assumed right ascension for the reference source 3C 273 and will have a systematic rotation compared to planetary ephemerides. Therefore, the new astrometric catalog should not be used for navigation as presented here, because it is necessary to make certain that the catalog used for a specific mission is generated using the same parameters (e.g., DSN station locations and precession and nutation constants) that are used by the navigators for that mission.

Compared to the last published catalog, there are 31 new sources within 20 deg of the ecliptic plane that have position errors less than five milliarcseconds and correlated flux densities above 0.2 Jy on at least one of the two DSN intercontinental baselines. Twenty-one of those sources are within 10 deg of the ecliptic. The radio sources in the catalog have been divided into several categories depending on their correlated flux densities on the DSN baselines. Sources in class 1 can be used with the current navigation VLBI system on baselines with two 34-m antennas, a 34-m and a 70-m antenna, or two 70-m antennas. Class 2 sources require at least one 70-m antenna, while class 3 sources require 70-m antennas on both ends of the baseline. Class 4 sources are too weak for navigation using two 70-m antennas and a 250-kHz-bandwidth system. The categorization, which is based on correlated flux densities measured between 1986 and 1988, has been made to facilitate source selection and the determination of antenna requirements.

The returns for a given effort are diminishing as weaker candidate sources are considered. Finding new sources in the region of the ecliptic plane in the same direction as the galactic center may require a new source survey rather than depending upon surveys that have been published already. Counts of sources as a function of correlated flux density indicate that ~70 more sources above 0.2-Jy correlated flux density should exist within 20 deg of the ecliptic plane. Such sources, if added to the VLBI catalog, could be observed for VLBI navigation with two 70-m antennas. However, examining about 1,000 sources to find the new objects would be a considerable undertaking.

The JPL VLBI catalog always will have gaping holes for navigation when the current 250-kHz-bandwidth system is used with two 34-m antennas. At present, usable navigation sources will be within 10 deg of a spacecraft in only 30 percent of the ecliptic; only 70 percent of the ecliptic has usable sources within 20 deg. One option is to use one or two 70-m antennas all the time, but those telescopes are heavily oversubscribed. Another option is to increase the observing bandwidth. Using the 15-year-old Mark II VLBI system, which samples at 4 Mbits/sec (effective bandwidth of 1.8 MHz) instead of the 0.5-Mbits/sec rate of the Block I system, would increase the sensitivity by a factor of more than 2.5. All category 3 sources would be reachable on a baseline between a 34-m and a 70-m antenna, and all Class 2 sources would be observable with two 34-m antennas. Using two 34-m antennas with this system, there would be a reference source within 10 deg of a spacecraft over 65 percent of the ecliptic, and a source within 20 deg over 98 percent of the ecliptic. For all class 3 sources to be reachable with two 34-m antennas, the bandwidth would have to be increased to $\sim$6.25 MHz, with a sampling rate of at least 12.5 Mbits/sec. Then, more than 90 percent of the ecliptic would have a usable source within 10 deg. Using these wider bandwidths in a real-time system would require higher rates of data transmission from the VLBI stations to JPL.

Acknowledgments

References

[1] O. J. Sovers, C. D. Edwards, C. S. Jacobs, G. E. Lanyi, K. M. Liewer, and R. N. Treuhaft, "Astrometric Results of 1978–1985 Deep Space Network Radio Interferometry: The JPL 1987-1 Extragalactic Source Catalog," *Astronomical Journal*, vol. 95, pp. 1647–1658, 1988.

[2] C. Ma, T. A. Clark, J. W. Ryan, T. A. Herring, I. I. Shapiro, B. E. Corey, H. F. Hinteregger, A. E. E. Rogers, A. R. Whitney, C. A. Knight, G. L. Lundqvist, D. B. Shaffer, N. R. Vandenberg, J. C. Pigg, B. R. Schupler, and B. O. Rönnäng, "Radio Source Positions from VLBI," *Astronomical Journal*, vol. 92, pp. 1020–1029, 1986.

[3] R. N. Treuhaft, "Deep Space Tracking in Local Reference Frames," *TDA Progress Report 42-94*, vol. April–June 1988, Jet Propulsion Laboratory, Pasadena, California, pp. 1–15, August 15, 1988.

[4] J. S. Ulvestad and R. P. Linfield, "The Search for Reference Sources for ΔVLBI Navigation of the Galileo Spacecraft," *TDA Progress Report 42-84*, vol. October–December 1985, Jet Propulsion Laboratory, Pasadena, California, pp. 152–163, February 15, 1986.

[5] A. E. Wehrle, D. D. Morabito, and R. A. Preston, "Very Long Baseline Interferometry Observations of 257 Extragalactic Radio Sources in the Ecliptic Region," *Astronomical Journal*, vol. 89, pp. 336–341, 1984.

[6] D. D. Morabito, A. E. Niell, R. A. Preston, R. P. Linfield, A. E. Wehrle, and J. Faulkner, "VLBI Observations of 416 Extragalactic Radio Sources," *Astronomical Journal,* vol. 91, pp. 1038–1050, 1986.

[7] R. A. Preston, D. D. Morabito, J. G. Williams, J. Faulkner, D. L. Jauncey, and G. D. Nicolson, "A VLBI Survey at 2.29 GHz," *Astronomical Journal,* vol. 90, pp. 1599–1641, 1985.

[8] A. P. Rao and S. Ananthakrishnan, "Interstellar Scattering in the Inner Parts of the Galaxy," *Nature,* vol. 312, pp. 707–711, 1984.

[9] J. B. Thomas, *Interferometry Theory for the Block II Processor,* JPL Publication 87-29, Jet Propulsion Laboratory, Pasadena, California, October 15, 1987.

[10] B. G. Clark "The NRAO Tape-Recorder Interferometer System," *Proc. IEEE,* vol. 61, pp. 1242–1248, 1973.

[11] A. E. E. Rogers, R. J. Cappallo, H. F. Hinteregger, J. I. Levine, E. F. Nesman, J. C. Webber, A. R. Whitney, T. A. Clark, C. Ma, J. Ryan, B. E. Corey, C. C. Counselman, T. A. Herring, I. I. Shapiro, C. A. Knight, D. B. Shaffer, N. R. Vandenberg, R. Lacasse, R. Mauzy, B. Rayhrer, B. R. Schupler, and J. C. Pigg, "Very Long Baseline Radio Interferometry: The Mark III System for Geodesy, Astrometry, and Aperture Synthesis," *Science,* vol. 219, pp. 51–54, 1983.

[12] S. D. Slobin, "DSS 14 64-Meter Antenna S- and X-Band Efficiency and System Noise Temperature Calibrations, September 1987," *TDA Progress Report 42-92,* vol. October–December 1987, Jet Propulsion Laboratory, Pasadena, California, pp. 138–146, February 15, 1988.

[13] S. D. Slobin and D. A. Bathker, "DSN 70-Meter Antenna X-Band Gain, Phase, and Pointing Performance, With Particular Application for Voyager 2 Neptune Encounter," *TDA Progress Report 42-95,* vol. July–September 1988, pp. 237–245, November 15, 1988.

[14] J. G. Bolton, A. Savage, and A. E. Wright, "The Parkes 2700 MHz survey (fourteenth part): Catalogue for declinations $-4°$ to $-15°$, right ascensions 10^h to 15^h," *Australian Journal of Physics Astrophysical Supplement,* no. 46, p. 1, 1979.

[15] J. J. Condon and J. J. Broderick, "A 1400 MHz Sky Survey. II. Confusion-limited Maps covering $19^h30^m < \alpha < 7^h30^m$, $-5° < \delta < +82°$," *Astronomical Journal,* vol. 91, pp. 1051–1057, 1986.

[16] C. L. Bennett, C. R. Lawrence, B. F. Burke, J. N. Hewitt, and J. Mahoney, "The MIT–Green Bank (MG) 5 GHz Survey," *Astrophysical Journal Supplement,* vol. 61, pp. 1–104, 1986.

[17] K. I. Kellermann and J. V. Wall, "Radio Source Counts and their Interpretation," in *International Astronomical Union Symposium No. 124, Observational Cosmology,* edited by A. Hewitt, G. Burbidge, and L. Fang, Dordrecht Reidel Publishing Company, pp. 545–564, 1987.

Table 1. Astrometric JPL VLBI catalog[a]

Name	Right Ascension h	Right Ascension m	Right Ascension s	Declination °	Declination ′	Declination ″	R.A. error s	Dec. error ″
P 0008 − 264	0	11	1.24699355	−26	12	33.3773551	0.00010644	0.0015781
P 0019 + 058	0	22	32.44118862	6	8	4.2720531	0.00003601	0.0012603
P 0048 − 09	0	50	41.31734533	−9	29	5.2057755	0.00005632	0.0014180
P 0104 − 408	1	6	45.10803890	−40	34	19.9565151	0.00012592	0.0013105
P 0106 + 01	1	8	38.77104811	1	35	0.3203449	0.00003232	0.0007163
P 0111 + 021	1	13	43.14504680	2	22	17.3176826	0.00010071	0.0017404
P 0112 − 017	1	15	17.09989294	−1	27	4.5744796	0.00003303	0.0007690
P 0113 − 118	1	16	12.52201531	−11	36	15.4319487	0.00004358	0.0009582
P 0119 + 11	1	21	41.59500938	11	49	50.4154942	0.00003038	0.0007081
GC 0119 + 04	1	21	56.86158102	4	22	24.7399107	0.00005209	0.0013681
DA 55	1	36	58.59476987	47	51	29.1017977	0.00004802	0.0005116
0146 + 056	1	49	22.37082174	5	55	53.5720621	0.00003300	0.0007601
P 0201 + 113	2	3	46.65701680	11	34	45.4119221	0.00003083	0.0007475
P 0202 + 14	2	4	50.41391519	15	14	11.0450538	0.00003467	0.0006642
0212 + 735	2	17	30.81344376	73	49	32.6235037	0.00010937	0.0003974
GC 0221 + 06	2	24	28.42814525	6	59	23.3439920	0.00003330	0.0013038
DW 0224 + 67	2	28	50.05164546	67	21	3.0322165	0.00012631	0.0008321
P 0229 + 13	2	31	45.89403472	13	22	54.7180082	0.00003289	0.0010830
CTD 20	2	37	52.40566460	28	48	8.9922817	0.00003301	0.0005215
GC 0235 + 16	2	38	38.93012333	16	36	59.2759391	0.00003493	0.0006428
OD 166	2	42	29.17087987	11	1	0.7295586	0.00003987	0.0008338
OD 094.7	2	59	27.07664169	7	47	39.6424948	0.00004394	0.0019742
OE 400	3	3	35.24220862	47	16	16.2776761	0.00004975	0.0005190
0306 + 102	3	9	3.62348204	10	29	16.3426808	0.00003299	0.0026601
0309 + 411	3	13	1.96212709	41	20	1.1849592	0.00004334	0.0008132
3C 84	3	19	48.16013053	41	30	42.1061371	0.00008238	0.0011983
0326 + 277	3	29	57.66936164	27	56	15.4992592	0.00003858	0.0011890
P 0332 − 403	3	34	13.65454152	−40	8	25.3957294	0.00014044	0.0014000
NRAO 140	3	36	30.10766072	32	18	29.3432486	0.00004501	0.0006706
CTA 26	3	39	30.93773041	−1	46	35.7999706	0.00003202	0.0009034
0342 + 147	3	45	6.41651123	14	53	49.5600248	0.00003363	0.0010192
P 0402 − 362	4	3	53.74977936	−36	5	1.9097062	0.00010031	0.0012249
GC 0406 + 12	4	9	22.00870257	12	17	39.8489955	0.00003703	0.0010056
P 0420 − 01	4	23	15.80070198	−1	20	33.0637547	0.00002786	0.0007633
VRO 41.04.01	4	23	56.00981686	41	50	2.7176069	0.00021967	0.0032146
P 0425 + 048	4	27	47.57029577	4	57	8.3305196	0.00012503	0.0021880
3C 120	4	33	11.09551075	5	21	15.6227035	0.00006154	0.0012917
P 0434 − 188	4	37	1.48270317	−18	44	48.6120617	0.00006570	0.0012561
P 0438 − 43	4	40	17.17988751	−43	33	8.6003713	0.00014003	0.0013208
0440 + 345	4	43	31.63521824	34	41	6.6646666	0.00003922	0.0007564
P 0446 + 11	4	49	7.67106994	11	21	28.5984746	0.00002903	0.0018032
P 0451 − 28	4	53	14.64620104	−28	7	37.3188681	0.00034099	0.0041906
0500 + 019	5	3	21.19711453	2	3	4.6786075	0.00002983	0.0017863
0454 + 844	5	8	42.36483468	84	32	4.5443577	0.00036133	0.0004369
P 0506 + 101	5	9	27.45707126	10	11	44.6020917	0.00002725	0.0011530
P 0507 + 17	5	10	2.36914548	18	0	41.5833675	0.00002938	0.0006610
P 0528 + 134	5	30	56.41678287	13	31	55.1506072	0.00003060	0.0006461
P 0537 − 441	5	38	50.36122088	−44	5	8.9347405	0.00014966	0.0013899
0536 + 145	5	39	42.36600089	14	33	45.5626621	0.00002762	0.0006572
0544 + 273	5	47	34.14897656	27	21	56.8449776	0.00005573	0.0016400
DA 193	5	55	30.80561462	39	48	49.1662319	0.00003830	0.0004967
0556 + 238	5	59	32.03315606	23	53	53.9275968	0.00002972	0.0005826
0600 + 177	6	3	9.13027327	17	42	16.8116293	0.00002997	0.0006438
P 0607 − 15	6	9	40.94970020	−15	42	40.6743233	0.00027504	0.0040739
3C 166	6	45	24.09952596	21	21	51.2023276	0.00002969	0.0006424
0657 + 172	7	0	1.52557647	17	9	21.7010705	0.00004964	0.0010824
P 0722 + 145	7	25	16.80776214	14	25	13.7479152	0.00002813	0.0019852
DW 0723 − 00	7	25	50.63992029	−0	54	56.5440972	0.00004696	0.0010124

[a] This catalog is a subset of the 1989-5 catalog, including all sources with formal declination errors of less than 5.0 milliarcseconds. Positions are given in J2000 coordinates, with the zero point of right ascension defined by the assumed right ascension of 3C 273.

Table 1 (contd)

Name	Right Ascension			Declination			R.A. error	Dec. error
	h	m	s	°	′	″	s	″
P 0727 − 11	7	30	19.11246024	−11	41	12.6005321	0.00003440	0.0009449
P 0735 + 17	7	38	7.39374592	17	42	18.9992145	0.00003255	0.0006931
P 0736 + 01	7	39	18.03391957	1	37	4.6186448	0.00010231	0.0038285
OI 363	7	41	10.70338957	31	12	0.2289329	0.00009196	0.0012888
DW 0742 + 10	7	45	33.05950366	10	11	12.6918275	0.00002903	0.0007084
GC 0743 + 25	7	46	25.87414169	25	49	2.1353629	0.00003262	0.0006390
B2 0745 + 24	7	48	36.10927896	24	0	24.1106879	0.00003958	0.0008046
P 0748 + 126	7	50	52.04575527	12	31	4.8275558	0.00003619	0.0007976
P 0754 + 100	7	57	6.64294522	9	56	34.8509802	0.00002652	0.0009451
OJ 425	8	18	15.99969677	42	22	45.4139981	0.00004286	0.0005609
P 0823 + 033	8	25	50.33837169	3	9	24.5196233	0.00002579	0.0007326
B2 0827 + 24	8	30	52.08616400	24	10	59.8208076	0.00003600	0.0005821
4C 71.07	8	41	24.36604803	70	53	42.1708564	0.00036869	0.0020193
OJ 287	8	54	48.87493186	20	6	30.6409927	0.00002475	0.0005294
OJ 499	9	3	3.99015987	46	51	4.1325722	0.00054797	0.0039037
P 0912 + 029	9	14	37.91348420	2	45	59.2452132	0.00005019	0.0009866
4C 39.25	9	27	3.01385886	39	2	20.8508520	0.00003726	0.0004605
1012 + 232	10	14	47.06547054	23	1	16.5697551	0.00004060	0.0006320
P 1034 − 293	10	37	16.07978339	−29	34	2.8134642	0.00008266	0.0011473
OL 064.5	10	41	17.16249455	6	10	16.9222264	0.00002980	0.0009321
3C 245	10	42	44.60589228	12	3	31.2591904	0.00035446	0.0047924
1044 + 719	10	48	27.62003187	71	43	35.9372599	0.00011409	0.0004905
P 1055 + 01	10	58	29.60522746	1	33	58.8229850	0.00002018	0.0007057
P 1104 − 445	11	7	8.69432359	−44	49	7.6190924	0.00018894	0.0015754
GC 1111 + 14	11	13	58.69511043	14	42	26.9511597	0.00003452	0.0006721
P 1123 + 26	11	25	53.71189910	26	10	19.9772741	0.00002800	0.0004920
P 1127 − 14	11	30	7.05268440	−14	49	27.3896707	0.00007075	0.0013349
GC 1128 + 38	11	30	53.28259214	38	15	18.5452991	0.00004249	0.0006856
P 1144 − 379	11	47	1.37079306	−38	12	11.0236144	0.00007819	0.0010893
P 1148 − 00	11	50	43.87085417	−0	23	54.2050281	0.00007624	0.0022801
P 1222 + 037	12	24	52.42189082	3	30	50.2925291	0.00003350	0.0009782
3C 273	12	29	6.69970000	2	3	8.5988392	0.00000001	0.0006671
3C 274	12	30	49.42341915	12	23	28.0421643	0.00030286	0.0040654
P 1244 − 255	12	46	46.80217065	−25	47	49.2896321	0.00004755	0.0009872
3C 279	12	56	11.16660613	−5	47	21.5265915	0.00002249	0.0008804
B2 1308 + 32	13	10	28.66380137	32	20	43.7811295	0.00003027	0.0004458
OP−322	13	16	7.98600558	−33	38	59.1718719	0.00013842	0.0015958
DW1335 − 12	13	37	39.78282936	−12	57	24.6935349	0.00002323	0.0008232
GC 1342 + 662	13	43	45.95944179	66	2	25.7429691	0.00011361	0.0007323
GC 1342 + 663	13	44	8.67949762	66	6	11.6417292	0.00008134	0.0004207
P 1349 − 439	13	52	56.53533280	−44	12	40.3888519˙	0.00019058	0.0015367
P 1354 + 19	13	57	4.43661980	19	19	7.3711230	0.00002427	0.0005085
OP−192	13	57	11.24503895	−15	27	28.7867430	0.00003011	0.0008814
OQ 208	14	7	0.39436580	28	27	14.6889018	0.00003172	0.0005476
GC 1418 + 54	14	19	46.59726856	54	23	14.7851817	0.00005389	0.0005101
OQ−151	14	32	57.69062126	−18	1	35.2493238	0.00027582	0.0038462
P 1445 − 16	14	48	15.05418706	−16	20	24.5487409	0.00003362	0.0008963
OR 103	15	4	24.97974565	10	29	39.1982308	0.00002066	0.0005423
P 1504 − 167	15	7	4.78702944	−16	52	30.2673226	0.00003536	0.0010599
P 1510 − 08	15	12	50.53293773	−9	5	59.8296275	0.00002424	0.0008074
P 1511 − 100	15	13	44.89334992	−10	12	0.2590722	0.00012513	0.0047020
P 1514 − 24	15	17	41.81336779	−24	22	19.4771955	0.00006876	0.0011368
P 1519 − 273	15	22	37.67599346	−27	30	10.7842172	0.00008423	0.0012447
P 1532 + 01	15	34	52.45359734	1	31	4.2075341	0.00002894	0.0007092
DW 1548 + 05	15	50	35.26917430	5	27	10.4485942	0.00002469	0.0006388
DW 1555 + 00	15	57	51.43393778	−0	1	50.4133609	0.00003074	0.0008196
DA 406	16	13	41.06412749	34	12	47.9077291	0.00003398	0.0005824
P 1614 + 051	16	16	37.55676335	4	59	32.7369010	0.00002445	0.0006393
GC 1633 + 38	16	35	15.49283800	38	8	4.4992151	0.00003668	0.0005022
NRAO 512	16	40	29.63260653	39	46	46.0280763	0.00004006	0.0005402
3C 345	16	42	58.80980000	39	48	36.9929752	0.00003562	0.0004583
OS 092	16	58	9.01137451	7	41	27.5425233	0.00004004	0.0009901

Table 1 (contd)

Name	Right Ascension			Declination			R.A. error	Dec. error
	h	m	s	°	'	"	s	"
DW 1656 + 05	16	58	33.44723638	5	15	16.4457268	0.00011546	0.0018022
P 1657 − 261	17	0	53.15421641	−26	10	51.7249256	0.00005629	0.0011049
OT−111	17	9	34.34542060	−17	28	53.3636920	0.00005597	0.0012250
GC 1717 + 17	17	19	13.04848761	17	45	6.4357837	0.00018765	0.0033162
NRAO 530	17	33	2.70579312	−13	4	49.5459665	0.00002905	0.0008033
OT 465	17	39	57.12882110	47	37	58.3606308	0.00004406	0.0006333
P 1741 − 038	17	43	58.85610106	−3	50	4.6152077	0.00002409	0.0006855
1749 + 701	17	48	32.83990518	70	5	50.7682029	0.00010839	0.0005487
OT 081	17	51	32.81849911	9	39	0.7294019	0.00002474	0.0007317
1803 + 784	18	0	45.68294237	78	28	4.0179481	0.00030408	0.0007011
3C 371	18	6	50.68020077	69	49	28.1086068	0.00008194	0.0004372
P 1821 + 10	18	24	2.85520298	10	44	23.7746943	0.00004006	0.0014917
OV−213	19	11	9.65297458	−20	6	55.1076354	0.00004556	0.0009498
OV−235	19	23	32.18985970	−21	4	33.3302802	0.00003863	0.0009280
OV−236	19	24	51.05617872	−29	14	30.1197921	0.00006617	0.0010194
OV 239.7	19	25	59.60523217	21	6	26.1630496	0.00002937	0.0005276
P 1936 − 15	19	39	26.65779536	−15	25	43.0564710	0.00003442	0.0008560
OV−198	20	0	57.09051289	−17	48	57.6703577	0.00003670	0.0008616
P 2008 − 159	20	11	15.71098648	−15	46	40.2508255	0.00003501	0.0008317
OW 637	20	22	6.68142238	61	36	58.8063153	0.00013980	0.0020267
OW 551	20	31	47.95843033	54	55	3.1481006	0.00032011	0.0036644
P 2029 + 121	20	31	54.99419610	12	19	41.3408484	0.00006625	0.0013675
B2 2113 + 29B	21	15	29.41332663	29	33	38.3684139	0.00003171	0.0006134
OX 036	21	23	44.51734537	5	35	22.0953806	0.00002753	0.0006091
P 2128 − 12	21	31	35.26172084	−12	7	4.7933609	0.00003429	0.0008040
P 2131 − 021	21	34	10.30957914	−1	53	17.2363608	0.00002918	0.0006818
P 2134 + 004	21	36	38.58638381	0	41	54.2145355	0.00002834	0.0006445
P 2145 + 06	21	48	5.45863130	6	57	38.6057827	0.00002729	0.0006223
OX 082	21	51	37.87535246	5	52	12.9567344	0.00004647	0.0010399
OX−192	21	58	6.28192609	−15	1	9.3260428	0.00014238	0.0020705
VRO 42.22.01	22	2	43.29124274	42	16	39.9817741	0.00003823	0.0004596
P 2216 − 03	22	18	52.03774097	−3	35	36.8783349	0.00003313	0.0008433
3C 446	22	25	47.25928239	−4	57	1.3886873	0.00003411	0.0008036
P 2227 − 08	22	29	40.08432367	−8	32	54.4322271	0.00003356	0.0007913
2229 + 695	22	30	36.46955494	69	46	28.0788256	0.00009468	0.0005378
CTA 102	22	32	36.40888182	11	43	50.9060834	0.00002704	0.0005475
GC 2234 + 28	22	36	22.47076608	28	28	57.4155420	0.00003138	0.0004683
OY−172.6	22	46	18.23197580	−12	6	51.2746746	0.00003672	0.0008401
P 2245 − 328	22	48	38.68575577	−32	35	52.1839028	0.00006021	0.0009986
3C 454.3	22	53	57.74787647	16	8	53.5628922	0.00003169	0.0006649
GC 2253 + 41	22	55	36.70769019	42	2	52.5347775	0.00005661	0.0010515
P 2254 + 024	22	57	17.56309267	2	43	17.5140935	0.00005252	0.0009038
GC 2318 + 04	23	20	44.85658844	5	13	49.9546884	0.00003016	0.0006805
P 2320 − 035	23	23	31.95371778	−3	17	5.0207566	0.00003543	0.0007714
P 2345 − 16	23	48	2.60855413	−16	31	12.0199908	0.00005820	0.0011185
P 2355 − 106	23	58	10.88243721	−10	20	8.6096896	0.00004540	0.0010260

Table 2. Correlated flux densities on Goldstone–Canberra baseline for all sources listed in Table 1 that have strengths determined from the experiments between 1986 and 1988[a]

Name	S-band Corr. flux density, Jy				No.	X-band Corr. flux density, Jy				No.
	Avg.	rms	Max	Min		Avg.	rms	Max	X_{min}	
P 0008−264	0.50	0.13	0.71	0.32	17	0.30	0.05	0.38	0.22	9
P 0019+058	0.20	0.02	0.23	0.18	4	0.15	0.04	0.19	0.10	4
P 0048−09	0.80	0.01	0.82	0.79	4	1.04	0.15	1.20	0.84	4
P 0104−408	1.25	0.15	1.50	1.03	13	2.33	0.13	2.56	2.21	5
P 0106+01	2.26	0.82	3.49	0.82	20	0.66	0.25	1.00	0.22	12
P 0112−017	1.07	0.01	1.08	1.07	3	1.16	0.08	1.25	1.06	3
P 0113−118	1.39	0.07	1.46	1.31	4	0.74	0.10	0.90	0.65	4
P 0119+11	0.18	0.05	0.25	0.14	3	0.34	0.06	0.42	0.30	3
DA 55	0.40	0.15	0.64	0.21	6	0.98	0.01	0.99	0.98	2
0146+056	0.81	0.02	0.84	0.79	3	0.37	0.02	0.39	0.35	3
P 0202+14	0.86	0.20	1.23	0.47	20	1.05	0.50	1.90	0.58	12
GC 0221+06	0.33	0.01	0.34	0.31	2	0.73	0.00	0.73	0.73	2
P 0229+13	0.86	0.04	0.91	0.81	3	0.62	0.03	0.65	0.58	3
CTD 20	1.08	0.25	1.52	0.57	19	1.68	0.56	2.42	0.95	11
GC 0235+16	1.39	0.17	1.75	1.17	19	0.89	0.31	1.26	0.31	11
OD 166	1.18	0.07	1.34	1.07	19	0.46	0.14	0.60	0.23	11
OE 400	1.41	0.32	1.92	0.81	12	1.25	0.63	2.10	0.42	6
0306+102	0.20	0.08	0.28	0.12	2	0.21	0.02	0.23	0.19	2
0309+411	0.33	0.02	0.35	0.30	4	0.35	0.14	0.48	0.15	3
3C 84	1.45	0.50	2.24	0.74	9	0.18	0.08	0.32	0.11	4
0326+277	0.17	0.03	0.22	0.12	6	0.21	0.04	0.25	0.13	5
P 0332−403	0.97	0.03	0.99	0.93	4	0.63	0.08	0.72	0.54	4
NRAO 140	1.00	0.27	1.46	0.76	4	0.37	0.16	0.62	0.19	4
CTA 26	1.20	0.29	1.63	0.79	14	0.69	0.29	1.02	0.37	6
0342+147	0.27	0.05	0.38	0.21	21	0.23	0.06	0.31	0.15	12
P 0402−362	0.47	0.08	0.60	0.31	12	1.63	0.22	2.00	1.33	8
GC 0406+12	0.66	0.09	0.78	0.45	19	0.10	0.02	0.13	0.07	10
P 0420−01	2.91	0.41	3.55	2.33	22	1.71	0.65	2.44	0.45	13
P 0425+048	0.24	0.05	0.30	0.13	20	0.21	0.04	0.26	0.13	12
3C 120	0.50	0.10	0.59	0.37	5	0.36	0.11	0.50	0.25	5
P 0434−188	1.00	0.06	1.14	0.89	22	0.49	0.09	0.63	0.35	12
P 0438−43	1.67	0.08	1.81	1.59	5	0.80	0.03	0.83	0.75	3
0440+345	0.77	0.06	0.87	0.66	9	0.13	0.07	0.23	0.06	3
P 0446+11	0.36	0.07	0.43	0.30	2	0.34	0.04	0.38	0.29	2
0500+019	0.88	0.04	0.93	0.84	2	0.36	0.01	0.37	0.34	2
P 0506+101	0.56	0.14	0.90	0.39	8	0.44	0.13	0.62	0.31	3
P 0507+17	0.20	0.06	0.32	0.09	11	0.32	0.11	0.53	0.22	6
P 0528+134	1.21	0.12	1.47	1.01	12	0.56	0.21	0.87	0.22	7
0536+145	0.44	0.04	0.52	0.37	11	0.31	0.10	0.43	0.15	6
P 0537−441	2.62	0.04	2.67	2.56	4	1.95	0.11	2.04	1.77	4
0544+273	0.16	0.03	0.22	0.13	11	0.20	0.10	0.31	0.07	5
DA 193	2.54	0.16	2.86	2.30	18	1.43	0.34	1.78	0.41	12
0556+238	0.50	0.16	0.72	0.17	13	0.50	0.24	0.77	0.11	7
0600+177	0.37	0.07	0.50	0.23	11	0.22	0.04	0.29	0.15	7
3C 166	0.24	0.10	0.34	0.07	4	0.00	0.00	0.00	0.00	0
0657+172	0.57	0.08	0.70	0.46	9	0.50	0.12	0.70	0.43	4
P 0722+145	0.43	0.03	0.46	0.40	3	0.00	0.00	0.00	0.00	0
DW 072300	0.37	0.24	0.71	0.18	3	0.22	0.15	0.43	0.08	3
P 0727−11	2.28	0.66	3.49	0.59	25	1.72	0.59	2.58	0.37	12
P 0735+17	0.60	0.12	0.81	0.41	13	0.66	0.25	1.29	0.47	8
P 0736+01	1.26	0.02	1.28	1.24	3	0.00	0.00	0.00	0.00	0
OI 363	1.73	0.11	1.87	1.53	6	0.41	0.19	0.69	0.17	6
DW 0742+10	1.01	0.07	1.12	0.91	11	0.82	0.05	0.89	0.76	5
GC 0743+25	0.45	0.01	0.46	0.44	4	0.00	0.00	0.00	0.00	0
B2 0745+24	0.83	0.23	1.16	0.52	7	0.82	0.00	0.82	0.82	1
P 0748+126	0.44	0.10	0.61	0.33	6	0.43	0.11	0.59	0.30	6
P 0754+100	0.33	0.01	0.35	0.31	3	0.00	0.00	0.00	0.00	0

[a] The "No." columns give total number of observations in the database. Ranges in flux density may be caused by variability from experiment to experiment, structure-induced differences among observations in a single experiment, or both.

Table 2 (contd)

Name	S-band Corr. flux density, Jy				No.	X-band Corr. flux density, Jy				No.
	Avg.	rms	Max	Min		Avg.	rms	Max	X_{min}	
OJ 425	1.40	0.10	1.50	1.24	6	0.53	0.00	0.53	0.53	1
P 0823+033	0.78	0.12	0.94	0.58	10	0.63	0.19	0.92	0.35	8
OJ 287	1.84	0.53	2.85	1.01	25	2.85	0.91	4.30	1.15	15
OJ 499	0.12	0.02	0.17	0.10	5	0.17	0.06	0.24	0.10	5
P 0912+029	0.25	0.01	0.26	0.24	2	0.00	0.00	0.00	0.00	0
4C 39.25	2.61	0.66	3.89	1.57	31	1.19	0.38	2.13	0.37	18
1012+232	0.54	0.05	0.61	0.50	3	0.00	0.00	0.00	0.00	0
P 1034−293	0.90	0.20	1.26	0.58	20	1.16	0.30	1.76	0.77	13
OL 064.5	0.52	0.08	0.67	0.41	8	0.74	0.17	0.89	0.40	8
P 1055+01	0.90	0.10	1.12	0.68	28	1.97	0.34	2.68	1.24	17
P 1104−445	1.77	0.10	1.88	1.63	6	0.57	0.08	0.65	0.46	6
P 1123+26	0.76	0.07	0.90	0.62	29	0.80	0.14	1.04	0.57	18
P 1127−14	0.55	0.19	0.82	0.32	7	0.14	0.02	0.16	0.12	3
GC 1128+38	0.64	0.06	0.76	0.57	8	0.32	0.04	0.38	0.28	8
P 1144−379	0.63	0.26	0.96	0.20	22	0.99	0.32	1.53	0.44	16
P 1222+037	0.91	0.07	1.03	0.80	9	0.52	0.07	0.58	0.45	2
3C 273	1.71	0.69	3.02	0.41	39	1.81 ·	0.44	2.74	0.89	22
P 1244−255	0.56	0.24	0.95	0.22	24	0.57	0.15	0.87	0.32	17
3C 279	1.21	0.44	1.87	0.26	11	0.96	0.24	1.32	0.64	6
B2 1308+32	0.95	0.29	1.42	0.37	37	1.17	0.70	2.34	0.33	22
OP−322	0.42	0.15	0.69	0.16	7	1.10	0.08	1.20	0.99	3
DW 1335−12	1.65	0.25	2.31	1.24	36	2.55	1.00	4.32	1.46	21
P 1349−439	0.38	0.05	0.44	0.31	5	0.33	0.03	0.36	0.31	2
OP−192	0.56	0.01	0.57	0.54	4	0.00	0.00	0.00	0.00	0
P 1354+19	0.88	0.15	1.18	0.59	34	1.02	0.32	1.45	0.52	21
OQ 208	0.22	0.05	0.31	0.16	10	0.13 ·	0.01	0.14	0.12	3
OQ−151	0.61	0.08	0.72	0.45	8	0.18	0.04	0.23	0.13	7
OR 103	1.29	0.24	1.78	0.71	29	0.82	0.24	1.43	0.37	17
P 1504−167	1.25	0.24	1.72	0.85	11	0.48	0.11	0.65	0.23	8
P 1510−08	1.32	0.19	1.77	1.08	24	1.38	0.44	2.63	0.85	12
P 1511−100	0.80	0.03	0.82	0.76	3	0.10	0.03	0.13	0.07	2
P 1514−24	0.37	0.08	0.48	0.30	3	0.34	0.03	0.37	0.30	2
P 1519−273	1.38	0.26	1.74	0.87	24	1.28	0.17	1.49	0.81	16
P 1532+01	0.56	0.03	0.59	0.51	3	0.33	0.00	0.34	0.33	2
DW 1548+05	0.96	0.06	1.04	0.89	3	0.59	0.03	0.62	0.56	2
DW 1555+00	0.30	0.05	0.41	0.20	28	0.35	0.05	0.42	0.22	16
DA 406	1.00	0.20	1.38	0.76	16	0.59	0.12	0.81	0.43	8
P 1614+051	0.36	0.01	0.37	0.34	2	0.25	0.00	0.25	0.25	1
GC 1633+38	2.04	0.19	2.24	1.71	12	1.70	0.32	2.16	1.16	9
NRAO 512	0.87	0.11	1.04	0.67	14	0.64	0.12	0.75	0.43	7
3C 345	4.28	0.84	5.70	3.03	21	3.67	0.31	4.03	3.12	11
OS 092	0.61	0.04	0.66	0.54	8	1.12	0.13	1.32	0.93	8
P 1657−261	0.80	0.34	1.46	0.47	9	1.56	0.50	2.47	1.14	9
OT−111	0.20	0.06	0.31	0.08	11	0.18	0.04	0.25	0.13	5
NRAO 530	0.68	0.31	1.34	0.28	32	1.57	0.75	2.56	0.14	22
OT 465	0.68	0.15	0.88	0.52	3	0.08	0.00	0.08	0.08	1
P 1741−038	1.13	0.24	1.58	0.75	28	0.75	0.13	0.91	0.49	18
OT 081	1.07	0.26	1.36	0.67	18	1.59	0.53	2.25	0.97	9
P 1821+10	0.70	0.13	0.85	0.39	9	0.22	0.06	0.28	0.10	9
OV−213	0.59	0.11	0.69	0.42	4	0.38	0.11	0.55	0.24	6
OV−235	0.86	0.13	1.23	0.73	21	0.99	0.13	1.30	0.76	16
OV−236	2.60	0.73	3.98	1.49	26	3.99	0.90	5.72	1.90	18
OV 239.7	0.39	0.07	0.49	0.27	19	0.32	0.10	0.44	0.12	8
P 1936−15	0.12	0.01	0.13	0.11	3	0.23	0.01	0.24	0.22	3
OV−198	1.60	0.26	2.15	1.06	27	1.60	0.44	2.21	0.75	16
P 2008−159	0.45	0.06	0.50	0.36	3	0.37	0.05	0.42	0.31	3
P 2029+121	0.34	0.02	0.37	0.32	6	0.48	0.09	0.59	0.34	6
B2 2113+29B	0.46	0.08	0.67	0.40	9	0.66	0.15	0.82	0.44	6
OX 036	2.73	0.03	2.77	2.69	3	0.77	0.05 ·	0.83	0.72	3
P 2128−12	0.27	0.02	0.28	0.24	3	0.67	0.07	0.77	0.60	3

Table 2 (contd)

Name	S-band Corr. flux density, Jy				No.	X-band Corr. flux density, Jy				No.
	Avg.	rms	Max	Min		Avg.	rms	Max	X_{min}	
P 2131−021	0.40	0.02	0.42	0.38	3	0.96	0.05	1.02	0.90	3
P 2134+004	0.65	0.20	0.97	0.32	16	1.20	0.29	1.73	0.79	12
P 2145+06	1.49	0.22	1.97	1.26	11	3.22	0.51	3.71	2.17	7
OX 082	0.59	0.06	0.69	0.45	13	0.25	0.02	0.27	0.19	7
OX−192	0.44	0.09	0.58	0.32	5	0.58	0.11	0.79	0.51	5
VRO 42.22.01	0.38	0.24	1.01	0.12	20	0.46	0.15	0.69	0.18	14
P 2216−03	1.37	0.19	1.62	1.08	9	0.50	0.14	0.70	0.38	3
3C 446	1.08	0.17	1.36	0.85	9	1.47	0.48	2.02	0.48	7
P 2227−08	0.40	0.05	0.44	0.33	3	1.13	0.10	1.24	1.00	3
CTA 102	1.89	0.20	2.46	1.54	19	0.75	0.14	1.10	0.52	16
GC 2234+28	1.55	0.23	1.96	1.11	20	0.41	0.13	0.73	0.23	16
OY−172.6	0.58	0.15	0.86	0.14	18	0.62	0.23	0.99	0.21	15
P 2245−328	0.52	0.20	0.86	0.17	25	0.32	0.06	0.39	0.14	14
3C 454.3	6.06	1.00	7.29	4.75	8	1.56	0.22	1.75	1.19	4
GC 2253+41	0.37	0.23	0.68	0.14	4	0.19	0.08	0.29	0.09	4
P 2254+024	0.24	0.02	0.27	0.23	3	0.30	0.02	0.32	0.27	3
GC 2318+04	0.79	0.01	0.81	0.78	3	0.61	0.04	0.66	0.57	3
P 2320−035	0.44	0.09	0.58	0.27	21	0.36	0.10	0.56	0.15	15
P 2345−16	1.36	0.47	1.88	0.28	16	0.56	0.29	0.94	0.22	8
P 2355−106	0.44	0.12	0.68	0.28	23	0.73	0.07	0.84	0.57	17

Table 3. Correlated flux densities on Goldstone–Madrid baseline for all sources listed in Table 1 that have strengths determined from the experiments between 1986 and 1988[a]

Name	S-band Corr. flux density, Jy				No.	X-band Corr. flux density, Jy				No.
	Avg.	rms	Max	Min		Avg.	rms	Max	X_{min}	
P 0019+058	0.26	0.05	0.34	0.17	8	0.29	0.06	0.40	0.20	6
P 0048−09	0.73	0.07	0.80	0.57	6	0.75	0.09	0.86	0.63	5
P 0106+01	2.33	0.57	3.44	1.42	14	0.45	0.12	0.65	0.21	12
P 0111+021	0.17	0.04	0.23	0.11	5	0.14	0.02	0.17	0.11	5
P 0112−017	0.95	0.04	1.01	0.88	7	0.60	0.10	0.77	0.43	7
P 0113−118	1.22	0.14	1.35	0.89	7	0.22	0.07	0.28	0.10	5
P 0119+11	0.59	0.06	0.72	0.51	8	0.64	0.12	0.85	0.48	8
GC 0119+04	0.56	0.05	0.62	0.50	5	0.86	0.18	1.15	0.60	5
DA 55	0.89	0.33	1.51	0.43	12	0.80	0.31	1.36	0.48	8
0146+056	0.82	0.05	0.90	0.75	7	0.14	0.02	0.18	0.12	7
P 0201+113	0.75	0.04	0.79	0.68	5	0.32	0.05	0.41	0.25	5
P 0202+14	0.68	0.23	1.08	0.32	15	0.88	0.40	1.48	0.30	11
0212+735	0.64	0.44	1.73	0.06	41	0.52	0.36	1.33	0.07	26
GC 0221+06	0.14	0.04	0.21	0.11	5	0.63	0.09	0.71	0.45	5
DW 0224+67	0.54	0.33	1.30	0.09	15	0.73	0.42	1.66	0.29	8
P 0229+13	0.80	0.08	0.93	0.70	4	0.62	0.12	0.79	0.46	4
CTD 20	1.31	0.41	2.21	0.83	13	2.34	0.78	3.71	1.36	10
GC 0235+16	1.44	0.69	2.63	0.72	14	1.19	0.86	2.83	0.20	8
OD 166	0.81	0.12	0.92	0.50	15	0.17	0.09	0.34	0.07	11
OE 400	1.24	0.15	1.48	0.91	15	0.88	0.18	1.18	0.63	10

[a] The "No." columns give total number of observations included in the database. Ranges in flux density may be caused by variability from experiment to experiment, structure-induced differences among observations in a single experiment, or both.

Table 3 (contd)

Name	S-band Corr. flux density, Jy				No.	X-band Corr. flux density, Jy				No.
	Avg.	rms	Max	Min		Avg.	rms	Max	X_{min}	
0306+102	0.19	0.07	0.26	0.08	5	0.21	0.03	0.24	0.16	5
0309+411	0.13	0.03	0.16	0.07	9	0.20	0.09	0.31	0.04	7
3C 84	1.80	0.91	2.88	0.44	6	0.54	0.10	0.68	0.42	4
0326+277	0.17	0.09	0.29	0.08	3	0.11	0.02	0.14	0.09	2
NRAO 140	0.42	0.04	0.47	0.38	3	0.29	0.00	0.29	0.29	1
CTA 26	1.45	0.20	1.70	1.18	8	0.56	0.13	0.71	0.32	6
0342+147	0.24	0.07	0.34	0.11	9	0.16	0.03	0.22	0.11	6
GC 0406+12	0.74	0.22	1.24	0.35	14	0.22	0.05	0.31	0.14	11
P 0420−01	3.32	0.37	3.84	2.68	13	2.03	0.63	3.05	1.10	7
P 0425+048	0.18	0.05	0.28	0.10	16	0.20	0.04	0.26	0.12	10
3C 120	0.29	0.05	0.33	0.24	2	0.00	0.00	0.00	0.00	0
P 0434−188	0.66	0.14	0.84	0.33	10	0.37	0.07	0.43	0.21	8
0440+345	0.82	0.07	0.90	0.75	2	0.35	0.00	0.35	0.35	1
P 0446+11	0.31	0.11	0.47	0.17	7	0.27	0.06	0.37	0.17	6
0454+844	0.32	0.08	0.47	0.16	33	0.13	0.06	0.25	0.04	22
0500+019	0.21	0.04	0.27	0.17	6	0.37	0.10	0.49	0.22	4
P 0506+101	0.55	0.11	0.70	0.38	7	0.36	0.07	0.48	0.27	6
P 0507+17	0.22	0.03	0.27	0.19	11	0.39	0.14	0.70	0.20	7
P 0528+134	1.65	0.21	2.01	1.37	9	0.98	0.47	1.70	0.44	4
0536+145	0.38	0.06	0.49	0.29	14	0.37	0.06	0.43	0.26	9
0544+273	0.20	0.07	0.32	0.08	15	0.29	0.11	0.54	0.14	10
DA 193	1.98	0.73	3.06	0.31	18	1.47	0.52	2.35	0.64	11
0556+238	0.65	0.13	0.81	0.49	11	0.59	0.05	0.65	0.52	7
0600+177	0.36	0.07	0.51	0.28	10	0.31	0.06	0.37	0.22	6
3C 166	0.30	0.07	0.38	0.16	11	0.23	0.05	0.29	0.16	7
0657+172	0.52	0.08	0.66	0.41	14	0.56	0.11	0.76	0.37	9
P 0722+145	0.29	0.06	0.35	0.20	3	0.18	0.05	0.23	0.14	2
DW 0723−00	0.29	0.00	0.29	0.29	1	0.20	0.00	0.20	0.20	1
P 0727−11	1.83	0.34	2.17	0.85	13	1.94	0.31	2.29	1.18	11
P 0735+17	0.81	0.15	1.09	0.58	7	0.86	0.32	1.24	0.46	3
P 0736+01	0.66	0.05	0.71	0.62	2	0.55	0.04	0.59	0.51	2
OI 363	1.71	0.15	2.00	1.50	6	0.37	0.21	0.58	0.16	2
DW 0742+10	2.71	0.24	3.19	2.31	10	0.45	0.06	0.53	0.34	6
GC 0743+25	0.42	0.02	0.45	0.40	4	0.20	0.02	0.22	0.19	2
B2 0745+24	0.39	0.20	0.71	0.04	8	0.44	0.16	0.63	0.23	4
P 0748+126	0.26	0.03	0.28	0.23	2	0.41	0.03	0.44	0.39	2
P 0754+100	0.50	0.06	0.56	0.43	3	0.29	0.01	0.30	0.27	2
OJ 425	1.12	0.11	1.33	0.93	13	0.41	0.08	0.53	0.27	7
P 0823+033	0.75	0.02	0.77	0.73	3	0.81	0.00	0.81	0.81	1
OJ 287	1.46	0.31	1.95	0.87	20	1.82	0.59	2.72	1.04	15
OJ 499	0.43	0.20	0.74	0.21	4	0.22	0.10	0.34	0.09	3
P 0912+029	0.43	0.02	0.45	0.40	3	0.36	0.02	0.38	0.34	2
4C 39.25	1.66	0.35	2.36	1.11	25	1.17	0.33	1.69	0.54	20
1012+232	0.20	0.07	0.28	0.10	4	0.50	0.10	0.63	0.38	3
OL 064.5	0.40	0.02	0.43	0.39	3	0.54	0.08	0.61	0.43	3
3C 245	0.24	0.01	0.26	0.23	3	0.06	0.00	0.07	0.06	3
1044+719	1.57	0.28	1.93	1.12	13	0.59	0.34	1.12	0.20	7
P 1055+01	0.61	0.10	0.83	0.41	17	1.41	0.28	2.12	1.01	12
P 1123+26	0.61	0.08	0.88	0.52	20	0.78	0.09	0.95	0.60	15
P 1127−14	1.13	0.23	1.37	0.74	7	0.15	0.02	0.18	0.12	4
GC 1128+38	0.57	0.11	0.69	0.32	7	0.28	0.10	0.39	0.08	6
P 1222+037	0.61	0.09	0.73	0.44	8	0.33	0.09	0.49	0.25	5
3C 273	3.79	0.60	4.53	2.07	21	1.58	0.64	2.60	0.83	13
P 1244−255	0.54	0.16	0.70	0.38	2	0.42	0.00	0.42	0.42	1
3C 279	3.23	0.24	3.51	2.83	6	1.81	0.52	2.56	1.22	5
B2 1308+32	0.60	0.23	0.94	0.27	27	0.40	0.15	0.80	0.16	18
DW 1335−12	2.17	0.63	3.16	0.89	12	2.20	0.83	3.87	1.11	9
GC 1342+663	0.48	0.07	0.64	0.39	32	0.14	0.06	0.25	0.04	22
OP−192	0.49	0.02	0.51	0.47	4	0.25	0.07	0.32	0.18	2
P 1354+19	0.65	0.13	0.90	0.40	26	0.52	0.19	0.89	0.25	17
OQ 208	0.63	0.03	0.68	0.58	9	0.35	0.06	0.45	0.28	6

Table 3 (contd)

Name	S-band Corr. flux density, Jy				No.	X-band Corr. flux density, Jy				No.
	Avg.	rms	Max	Min		Avg.	rms	Max	X_{min}	
GC 1418+54	0.75	0.19	1.18	0.38	21	0.43	0.23	0.81	0.05	13
P 1445−16	0.61	0.00	0.61	0.61	1	0.16	0.00	0.16	0.16	1
OR 103	1.23	0.26	1.84	0.90	25	0.43	0.12	0.77	0.23	17
P 1504−167	1.14	0.81	2.28	0.51	3	0.18	0.07	0.27	0.12	3
P 1510−08	0.98	0.52	2.19	0.44	10	1.78	0.19	2.02	1.58	4
P 1511−100	0.72	0.13	0.94	0.62	5	0.08	0.01	0.09	0.07	2
P 1532+01	0.47	0.04	0.54	0.42	7	0.21	0.07	0.29	0.08	5
DW 1548+05	1.49	0.17	1.82	1.30	6	0.77	0.19	0.98	0.50	4
DW 1555+00	0.26	0.04	0.35	0.19	19	0.25	0.07	0.38	0.13	15
DA 406	1.36	0.22	1.77	0.95	16	0.93	0.22	1.23	0.69	9
P 1614+051	0.52	0.02	0.56	0.48	6	0.24	0.03	0.28	0.20	5
GC 1633+38	1.72	0.25	2.13	1.33	20	0.88	0.38	1.80	0.31	11
NRAO 512	0.80	0.14	0.99	0.63	15	0.83	0.27	1.28	0.37	7
3C 345	3.20	0.48	4.61	2.24	41	2.17	0.65	4.13	1.36	16
OS 092	0.32	0.04	0.39	0.25	11	0.35	0.06	0.44	0.25	10
DW 1656+05	0.47	0.03	0.50	0.44	2	0.31	0.00	0.31	0.31	2
OT−111	0.21	0.09	0.35	0.10	5	0.17	0.04	0.23	0.14	3
NRAO 530	2.36	0.37	3.01	1.82	19	1.68	0.44	2.39	1.05	10
OT 465	0.67	0.14	0.81	0.24	17	0.30	0.17	0.53	0.05	14
P 1741−038	1.58	0.21	2.03	1.16	30	1.43	0.23	1.86	0.92	17
1749+701	0.20	0.06	0.33	0.13	10	0.11	0.02	0.15	0.08	8
OT 081	1.01	0.17	1.34	0.71	18	1.35	0.23	1.78	0.80	16
1803+784	1.24	0.09	1.33	1.15	2	1.71	0.15	1.86	1.57	2
3C 371	0.53	0.15	0.92	0.35	40	0.36	0.19	1.02	0.10	27
P 1821+10	0.83	0.10	0.95	0.60	16	0.32	0.04	0.40	0.28	7
OV−213	1.77	0.29	2.03	1.07	8	0.91	0.13	1.12	0.71	7
OV−235	1.36	0.41	1.81	0.75	7	1.05	0.35	1.46	0.58	6
OV 239.7	0.33	0.07	0.45	0.22	14	0.28	0.18	0.64	0.07	12
P 1936−15	0.27	0.03	0.32	0.22	7	0.22	0.05	0.26	0.13	5
OV−198	1.83	0.26	2.27	1.40	10	1.10	0.27	1.53	0.74	8
2008−159	0.81	0.04	0.88	0.76	5	0.66	0.05	0.71	0.58	5
OW 637	0.50	0.08	0.65	0.35	8	0.47	0.19	0.80	0.26	5
P 2029+121	0.58	0.06	0.66	0.49	10	0.19	0.06	0.29	0.13	8
OW 551	0.53	0.09	0.69	0.45	4	0.08	0.02	0.11	0.06	2
B2 2113+29B	0.75	0.15	0.96	0.41	12	0.56	0.12	0.80	0.36	9
OX 036	2.40	0.16	2.64	2.18	7	0.61	0.12	0.78	0.42	7
P 2128−12	1.08	0.07	1.17	0.95	5	0.55	0.13	0.77	0.39	5
P 2131−021	0.31	0.05	0.42	0.26	7	0.93	0.11	1.10	0.76	6
P 2134+004	2.34	0.33	2.92	1.83	17	1.12	0.34	1.84	0.48	14
P 2145+06	0.89	0.11	1.05	0.73	6	3.17	0.49	3.83	2.41	6
OX 082	0.60	0.06	0.68	0.47	9	0.21	0.03	0.26	0.15	7
VRO 42.22.01	1.68	0.81	3.21	0.84	21	1.19	0.48	2.05	0.59	14
P 2216−03	1.85	0.12	2.03	1.62	10	0.74	0.11	0.89	0.53	8
3C 446	1.37	0.03	1.41	1.34	2	1.76	0.19	1.95	1.57	2
P 2227−08	0.78	0.05	0.87	0.74	4	1.05	0.20	1.30	0.73	4
2229+695	1.05	0.12	1.25	0.86	13	0.35	0.14	0.62	0.13	9
CTA 102	0.80	0.57	2.19	0.13	22	0.42	0.17	0.74	0.06	17
GC 2234+28	1.22	0.22	1.58	0.38	24	0.42	0.18	0.71	0.06	19
OY−172.6	1.00	0.14	1.17	0.73	8	0.80	0.11	0.97	0.61	6
3C 454.3	4.98	1.62	6.97	1.94	12	1.57	1.04	3.10	0.16	9
GC 2253+41	1.06	0.11	1.15	0.91	3	0.31	0.07	0.39	0.24	2
P 2254+024	0.28	0.03	0.31	0.23	6	0.20	0.04	0.25	0.14	6
GC 2318+04	0.66	0.06	0.77	0.60	7	0.42	0.06	0.51	0.34	7
P 2320−035	0.55	0.04	0.63	0.44	15	0.35	0.10	0.56	0.18	13
P 2345−16	0.58	0.22	0.95	0.22	11	0.50	0.13	0.73	0.37	9
P 2355−106	0.59	0.18	0.86	0.30	18	0.56	0.09	0.74	0.42	12

Table 4. Correlated flux density classes for all sources listed in Table 1[a]

Name	Goldstone–Canberra S	Goldstone–Canberra X	Goldstone–Canberra S/X	Goldstone–Madrid S	Goldstone–Madrid X	Goldstone–Madrid S/X
P 0008–264	3	3	3			—
P 0019+058	4	4	4	3	3	3
P 0048–09	2	1	2	2	2	2
P 0104–408	1	1	1			—
P 0106+01	1	2	2	1	2	2
P 0111+021			(4)	4	4	4
P 0112–017	1	1	1	2	2	2
P 0113–118	1	2	2	1	4	4
P 0119+11	4	3	4	2	2	2
GC 0119+04			(3)	2	2	2
DA 55	3	1	3	2	2	2
0146+056	2	3	3	2	4	4
P 0201+113			(3)	2	3	3
P 0202+14			(3)	3	2	3
0212+735			—	3	3	3
GC 0221+06	3	2	3	4	2	4
DW 0224+67			—	3	2	3
P 0229+13	2	2	2	2	2	2
CTD 20	2	1	2	1	1	1
GC 0235+16	1	2	2	2	2	2
OD 166	1	3	3	2	4	4
OD 094.7			(3)			(3)
OE 400	1	2	2	1	2	2
0306+102	4	4	4	4	3	4
0309+411	3	4	4	4	4	4
3C 84	1	4	4	1	2	2
0326+277	4	4	4	4	4	4
P 0332–403	2	2	2			—
NRAO 140	2	3	3	3	3	3
CTA 26	2	2	2	1	2	2
0342+147	3	4	4	3	4	4
P 0402–362	3	1	3			—
GC 0406+12	2	4	4	2	4	4
P 0420–01	1	1	1	1	1	1
VRO 41.04.01			(3)			(3)
P 0425+048	3	4	4	4	4	4
3C 120		3	3	3	3	(4)
P 0434–188	2	2	2	2	3	3
P 0438–43	1	2	2			—
0440+345	2	4	4	2		(4)
P 0446+11	3	3	3	3		(3)
P 0451–28			(4)			—
0500+019		3	(4)	4	3	4
0454+844			—	3	4	4
P 0506+101	3	3	3	3	3	3
P 0507+17	4		4	3	3	3
P 0528+134	1	3	3	1	2	2
P 0537–441	1	1	1			—
0536+145	3	3	3	3	3	3
0544+273	4	4	4	4	3	4
DA 193	1	1	1	1	1	1
0556+238	3	2	3	2	2	2
0600+177	3	4	4	3	3	3
P 0607–15			(4)			(4)
3C 166			(4)	3	4	4
0657+172	3	2	3	3	2	3
P 0722+145	3		(4)	3	4	4
DW 0723–00	4	4	4	3	3	3
P 0727–11	1	1	1	1	1	1
P 0735+17	2	2	2	2	2	2
P 0736+01	1		(2)	2	2	2
OI 363	1	3	3	1	3	3
DW 0742+10	2	2	2	1	2	2
GC 0743+25	3		(3)	3	3	3
B2 0745+24	2		(2)	3	3	3
P 0748+126	3	3	3	3	2	3
P 0754+100	3		(3)	3	3	3
OJ 425	1	2	2	1	3	3
P 0823+033	2	2	2	2	1	2
B2 0827+24			(3)			(3)
4C 71.07			—			(4)
OJ 287	1	1	1	1	1	1
OJ 499	4	4	4	3	4	4
P 0912+029	3		(3)	3	3	3
4C 39.25	1	1	1	1	1	1
1012+232	2		(3)	4	3	4
P 1034–293	2	1	2			—
OL 064.5	3	2	3	3	2	3
3C 245			(3)	3		(3)
1044+719			—	1	3	3
P 1055+01	2	1	2	2	1	2
P 1104–445	1	2	2			—
GC 1111+14			(4)			(4)
P 1123+26	2	2	2	2	2	2
P 1127–14	3	4	4	2	4	4
GC 1128+38	2	3	3	2	3	3
P 1144–379	3	2	3			—
P 1148–00			(4)			(4)
P 1222+037	2	2	2	2	3	3
3C 273	1	1	1	1	1	1
3C 274			(3)			(3)
P 1244–255	3	2	3	3	2	3
3C 279	1	2	2	1	1	1
B2 1308+32	2	2	2	3	3	3
OP-322	3	1	3			—
DW 1335–12	1	1	1	1	1	1
GC 1342+662			—			(4)
GC 1342+663			—	3	4	4
P 1349–439	3	3	3			—
P 1354+19	2	2	2	2	3	3
OP-192	2		(2)	3	4	4
OQ 208	4	4	4	2	3	3
GC 1418+54			—	2	3	3
OQ-151	2	4	4			(4)
P 1445–16			—	2	4	4
OR 103	1	2	2	1	3	3
P 1504–167	1	2	2	2	4	4
P 1510–08	1	1	1	2	1	2
P 1511–100	2	4	4	2	4	4
P 1514–24	3	3	3			(3)

[a] Class 1 sources are observable with two 34-m antennas, class 2 sources require at least one 70-m antenna, and class 3 sources require two 70-m antennas for observation with the navigation VLBI system. Class 4 sources are too weak even for two 70-m antennas. Values are given in parentheses for sources with insufficient data in the 1986–1988 period. Dashes indicate sources that are not visible on the specified baseline.

Table 4 (contd)

Name	Goldstone–Canberra			Goldstone–Madrid			Name	Goldstone–Canberra			Goldstone–Madrid		
	S	X	S/X	S	X	S/X		S	X	S/X	S	X	S/X
P 1519–273	1	1	1			—	P 2008–159	3	3	3	2	2	2
P 1532+01			(3)	3	3	3	OW 637			—	3	3	3
DW 1548+05	2	2	2	1	2	2	OW 551			—	3		(3)
DW 1555+00	3	3	3	3	3	3	P 2029+121	3	3	3	2	4	4
DA 406	2	2	2	1	2	2	B2 2113+29B	3	2	3	2	2	2
P 1614+051	3	3	3	2	3	3	OX 036	1	2	2	1	2	2
GC 1633+38	1	1	1	1	2	2	P 2128–12	3	2	3	1	2	2
NRAO 512	2	2	2	2	2	2	P 2131–021	3	1	3	3	1	3
3C 345	1	1	1	1	1	1	P 2134+004	2	1	2	1	1	1
OS 092	2	1	2	3	3	3	P 2145+06	1	1	1	2	1	2
DW 1656+05			(3)	3	3	3	OX 082	2	3	3	2	3	3
1657–261	2	1	2			—	OX–192	3	2	3			(3)
OT–111	4	4	4	4	4	4	VRO 42.22.01	3	3	3	1	2	2
GC 1717+17			(3)			(3)	P 2216–03	1	3	3	1	2	2
NRAO 530	3	1	3	1	1	1	3C 446	2	1	2	1	1	1
OT 465	2	4	4	2	4	4	P 2227–08	3	1	3	2	1	2
P 1741–038	1	2	2	1	1	1	2229+695			—	2	3	3
1749+701			—	4	4	4	CTA 102	1	3	3	3	3	3
OT 081	2	1	2	2	1	2	GC 2234+28	1	3	3	1	3	3
1803+784			—	1	1	1	OY–172.6	2	3	3	2	2	2
3C 371			—	3	3	3	P 2245–328	3	3	3			—
P 1821+10	2	3	3	2	3	3	3C 454.3	1	1	1	1	1	1
OV–213	2	3	3	1	2	2	GC 2253+41	4	4	4	2	3	3
OV–235	2	2	2	2	2	2	P 2254+024	3	3	3	3	4	4
OV–236	1	1	1			—	GC 2318+04	2	2	2	2	3	3
OV 239.7	3	3	3	3	4	4	P 2320–035	3	3	3	2	3	3
P 1936–15	4	3	4	3	3	3	P 2345–16	1	3	3	3	2	3
OV–198	1	1	1	1	1	1	P 2355–106	3	2	3	3	2	3

Table 5. Portion of global source-finding list for ecliptic sources. The most accurate positions available in the 1950 coordinate system are given.[a]

Source	Right Ascension			Declination			Total Flux Density, Jy				Survey	VLBI	CEI	Notes
	h	m	s	°	′	″	5 GHz	2.7 GHz	1.4 GHz	0.4 GHz				
0000−177	00	00	48.6	−17	43	57.	0.95	1.37	2.2		6	N	N	
0001+128	00	01	07.06	12	49	58.1	0.41	0.66	1.12		20	N	Y	
0002+125	00	02	24.74	12	31	32.5	0.56		1.70		8	N	Y	
0003+158	00	03	26.7	15	52	38.	0.43	0.7	0.9	2.7	20	N	Y	
0003−066	00	03	40.293	−06	40	17.30	1.58	1.46	1.53		3	Y	Y	
0003−003	00	03	48.8	−00	21	06.	1.41	2.40	3.36		8	Y	Y	3C2
0005−199	00	05	43.8	−19	56	30.	0.25	0.45	0.53		3	N	N	
0005−062	00	05	55.8	−06	15	25.	0.33	0.68	1.2		6	N	N	
0007+124	00	07	18.5	12	28	40.	0.68	1.2	1.9		22	N	Y	
0007+106	00	07	57.9	10	41	30.	0.47		.0.34			Y	Y	
0007+171	00	07	59.383	17	07	37.50	0.92	0.91	0.83		8	Y	Y	
0009+081	00	09	01.7	08	07	14.6	0.36	0.49			8	N	Y	
0010+005	00	10	37.40	00	35	09.2	0.50	0.95	1.53		10	Y	Y	3C5
0011−046	00	11	20.64	−04	40	32.7	0.41	0.21			6	Y	N	
0011−096	00	11	24.3	−09	36	38.	0.26	0.40	0.82		6	N	N	
0011+054	00	11	29.3	05	28	46.	0.47	0.70	1.29		20	N	N	
0012−184	00	12	30.4	−18	28	48.	0.42	0.48	0.52		6	N	N	
0013−197	00	13	28.4	−19	45	56.	0.27	0.48	0.69		6	N	N	
0013−005	00	13	37.347	−00	31	52.50	0.68	0.87	0.91		10	Y	Y	

[a] VLBI and CEI indicate whether or not a source has been observed with VLBI or connected-element interferometry. List was last updated 14 July 1989. Selection criteria as of 18 January 1988:

(1) All sources within 20 deg of ecliptic fulfilling the following:
  (a) Five-GHz flux density above 250 mJy in MIT-GB survey.
  (b) Five-GHz flux density above 250 mJy in Parkes surveys, or if no 5-GHz flux density is given in Parkes survey or other surveys such as MIT-GB survey, flux density above 250 mJy at 2.7 GHz.
  (c) Any S-/X-band VLBI observations, regardless of total flux density.
  (d) Five-GHz flux density above 250 mJy in other surveys (e.g., S surveys).

(2) Exceptions:
  (a) Declinations generally limited to +40 deg in north and to −35 deg in south.
  (b) Some sources slightly more than 20 deg from ecliptic are included if they have lots of potential or are in otherwise empty regions (e.g., 0420−014). A few sources outside of +40-deg or −35-deg declination are also included.
  (c) Sources observed specifically for ecliptic reasons (e.g., Phobos lander frame-tie candidates) are included even if their flux densities are below the selection limit.
  (d) Sources in selected regions chosen from Condon−Broderick 1.4-GHz survey are included down to 200 mJy at 1.4 GHz. Even those sources which turn out to have 5-GHz flux densities below 250 or 300 mJy are still included.
  (e) Of course, some other random sources are included for various reasons.
  (f) The 0.4-GHz column is fairly incomplete, especially in cases where there are fluxes at two or three of the higher frequencies. In such cases, it was usually decided that it was not worth the trouble of finding a flux density at the lowest frequency, since it would add no useful information.
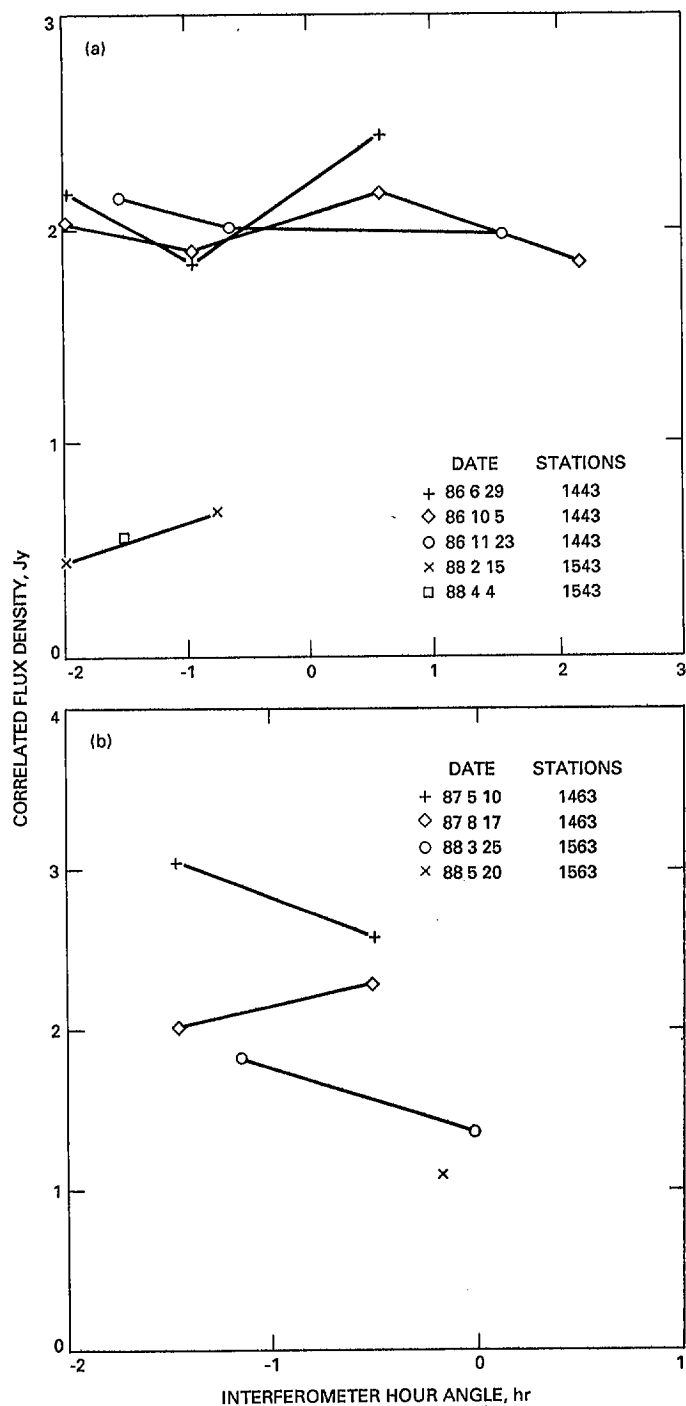
Fig. 1. Correlated flux density versus hour angle for P0420-014 at X-band: (a) on the California–Australia baseline, (b) on the California–Spain baseline.
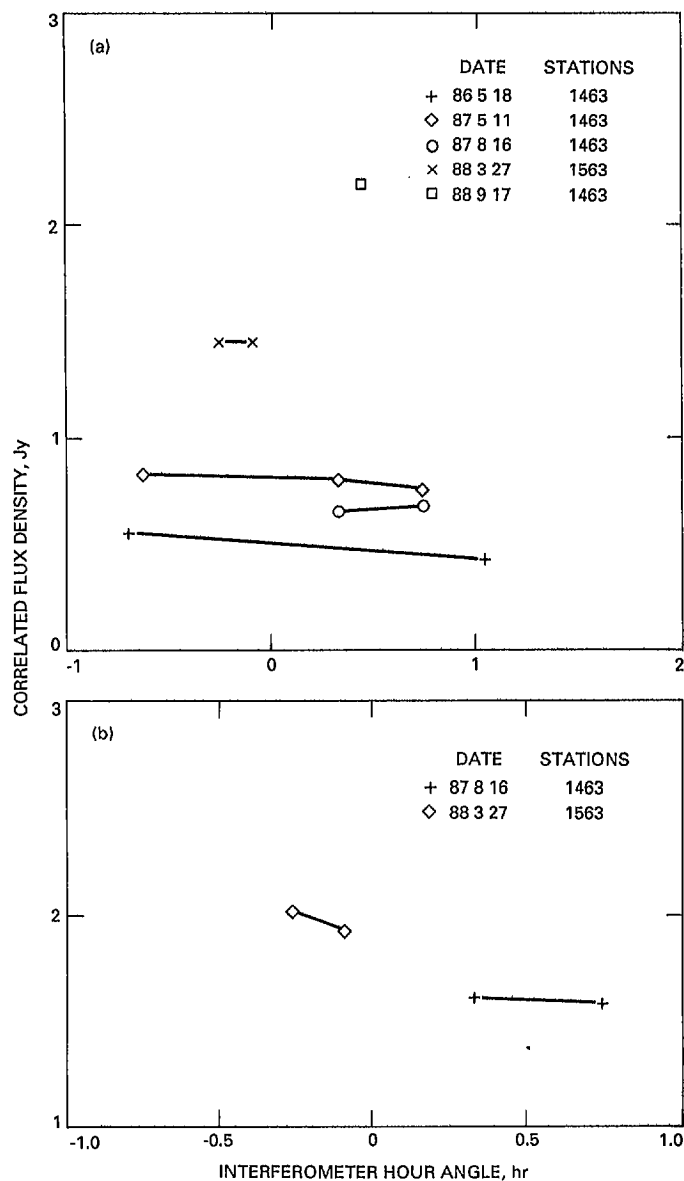

Fig. 2. Correlated flux density versus hour angle for P1510-08: (a) at S-band, (b) at X-band.
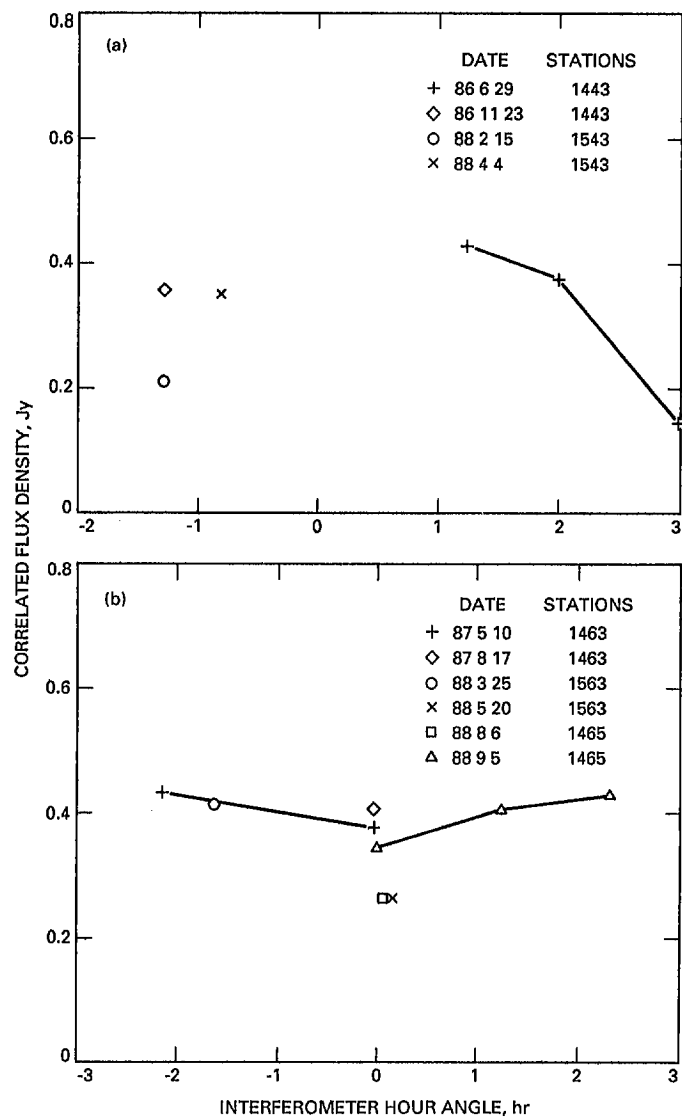
Fig. 3. Correlated flux density versus hour angle at X-band for 0536+145: (a) on the California–Australia baseline, (b) on the California–Spain baseline.
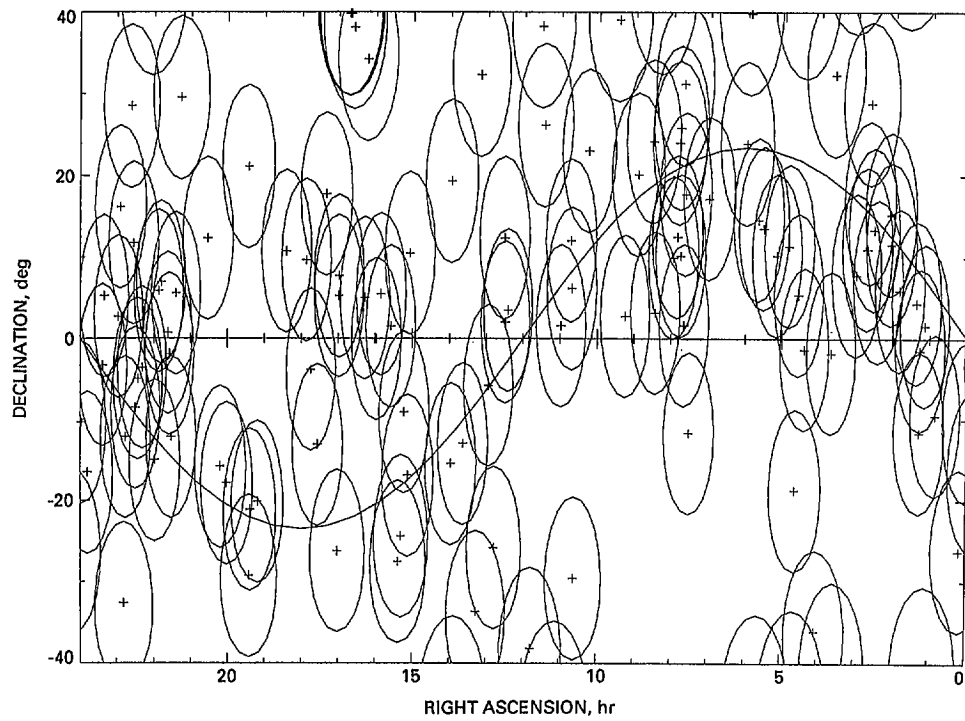
Fig. 4. Class 1, 2, and 3 sources on the California–Australia baseline are plotted on a pro-
jection of a portion of the celestial sphere. Circles of 10-degree radius are plotted at each
source position, and the ecliptic plane is shown as the sinusoidal curve. These sources have
correlated flux densities of at least 0.2 Jy at both S- and X-bands.
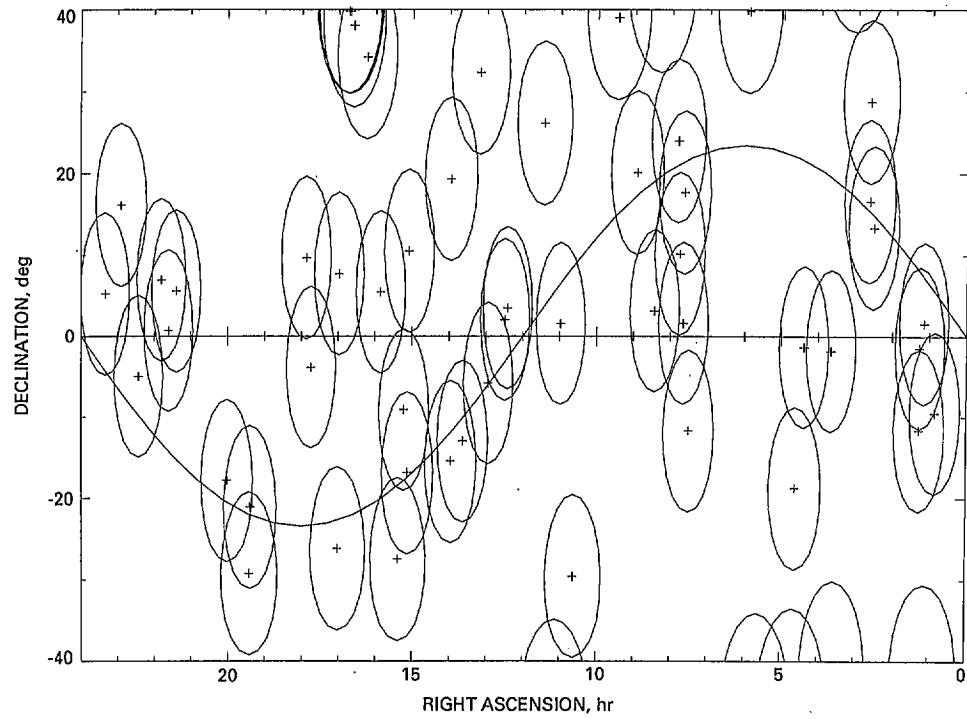
Fig. 5. Class 1 and class 2 sources on the California–Australia baseline are plotted on a projection of a portion of the celestial sphere. Circles of 10-degree radius are plotted at each source position. These sources have correlated flux densities of at least 0.5 Jy at S-band and 0.4 Jy at X-band. Similar to Fig. 4.
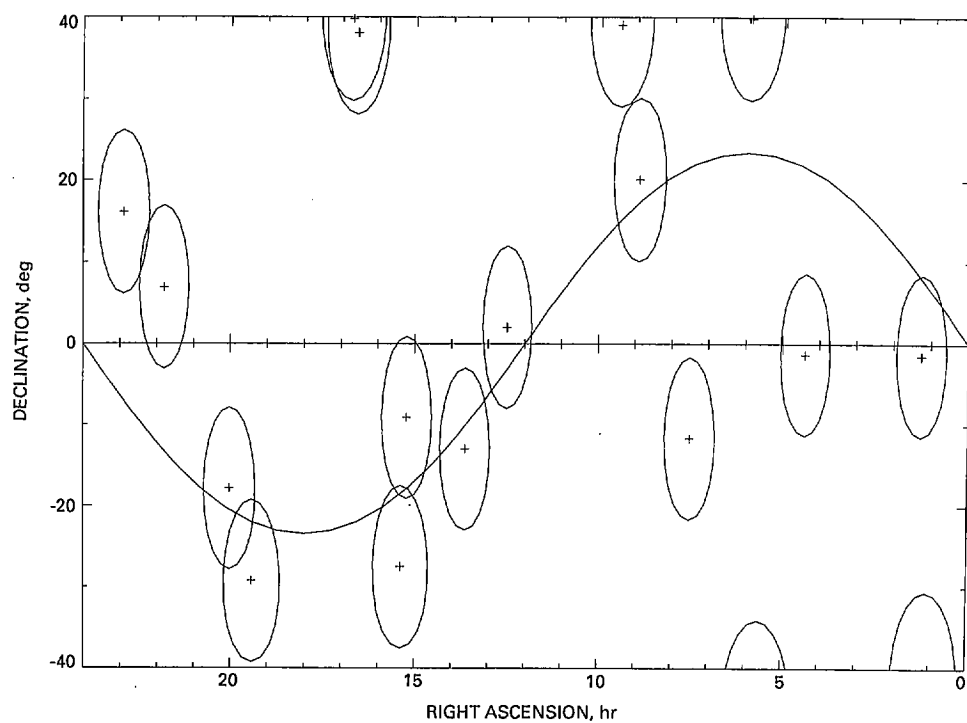
Fig. 6. Class 1 sources on the California–Australia baseline are plotted on a projection of a portion of the celestial sphere. These sources have correlated flux densities of at least 1.0 Jy at S band and 0.8 Jy at X-band. Similar to Fig. 4.
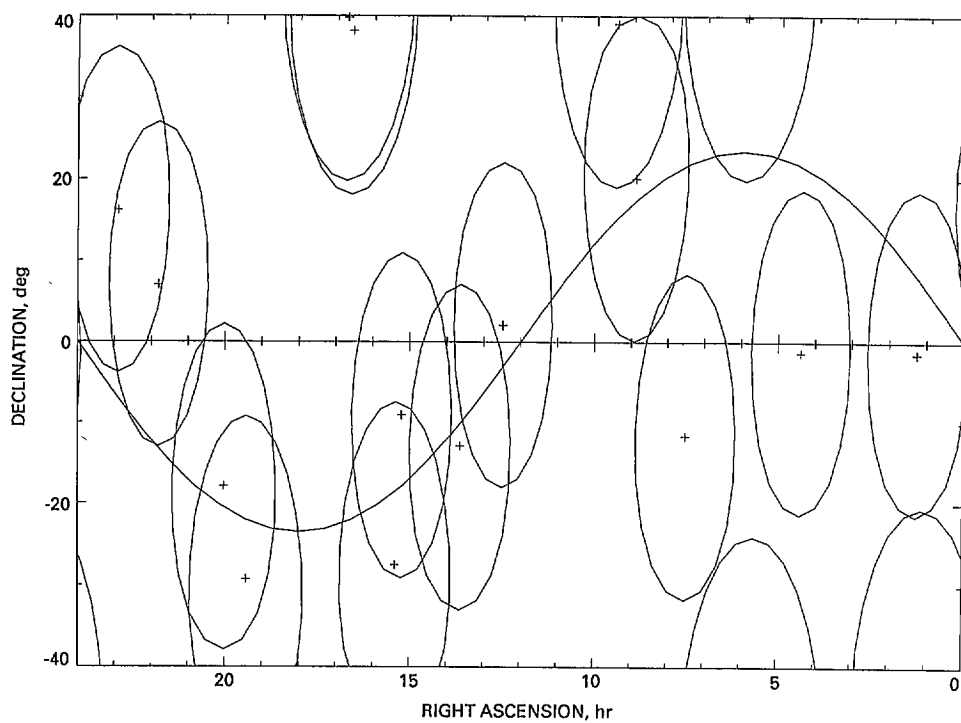

Fig. 7. Circles of radius 20 degrees are plotted at the position of each class-1 source on the California–Australia baseline. Similar to Fig. 4.
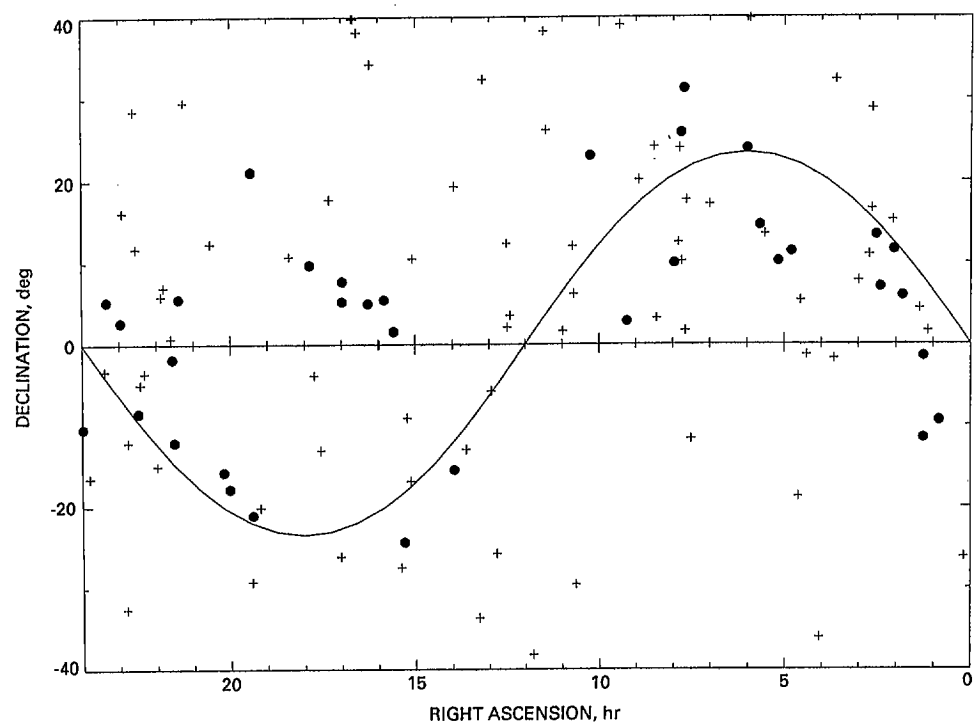
Fig. 8. Plot of each source in classes 1, 2, or 3 on the California–Australia baseline. Each new source is indicated by a ● and each old source is indicated by a +.